Bound states at the interface between antiferromagnets and superconductors

Brian M. Andersen,[1] I. V. Bobkova,[2] P. J. Hirschfeld,[1] and Yu. S. Barash[2]
[1]*Department of Physics, University of Florida, Gainesville, Florida 32611-8440, USA*
[2]*Institute of Solid State Physics, Chernogolovka, Moscow reg. 142432, Russia*
(Received 8 August 2005; published 16 November 2005)

We present a detailed theoretical investigation of interfaces and junctions involving itinerant antiferromagnets. By solving the Bogoliubov–de Gennes equations with a tight-binding model on a square lattice, we study both the self-consistent order parameter fields proximate to interfaces between antiferromagnets (AF) and *s*-wave (sSC) or *d*-wave (dSC) superconductors, the dispersion of quasiparticle subgap states at interfaces and interlayers, and the local density of states (LDOS) as a function of distance from the interface. In addition, we present the quasiclassical approach to interfaces and junctions involving itinerant antiferromagnets developed in an earlier paper. Analytical results are in excellent agreement with what we obtain numerically. Strong effects of pair breaking in the presence of low-energy interface Andreev states are found in particular for AF/sSC interfaces when interface potentials are not too high. Potential barriers induce additional extrema in the dispersive quasiparticle spectra with corresponding peaks in the LDOS. Discrete quasiparticle dispersive levels in AF–normal metal (*N*)–AF systems are found to depend strongly on the misorientation angle of the magnetizations in the two antiferromagnets.

DOI: 10.1103/PhysRevB.72.184510 PACS number(s): 74.45.+c, 74.50.+r

I. INTRODUCTION

Interfaces of magnetic materials with normal metals and superconductors have attracted much attention in recent years because they can strongly influence properties of mesoscopic and nanoscopic systems, and may play an important role in compounds with competing magnetic and superconducting ordering. Hybrid superconducting systems involving ferromagnets and/or antiferromagnets manifest unusual properties associated with spin and orbital effects, and are of both fundamental interest and importance for technological applications. Ferromagnetic layers can spin polarize quasiparticle currents and Zeeman split surface densities of states with possible applications in spintronics.[1] Superconductor-ferromagnet-superconductor (SC/F/SC) junctions have been shown to display 0-π transitions with varying temperature, width, or orientational structure of the magnetization of the ferromagnetic interlayer.[2–10]

There are also many situations of fundamental and practical interest which involve interfaces with antiferromagnets. In particular, many of the properties of high-temperature superconducting (HTS) cuprate materials are thought to result from a competition between antiferromagnetic and superconducting order, and there are many naturally occurring situations and possible devices which might involve such boundaries. These include interfaces of insulating and highly doped cuprates or superconductor-antiferromagnet-superconductor (SC/AF/SC) junctions,[11,12] HTS grain boundaries,[13] where antiferromagnetism may play a role as a surface state, and the antiferromagnetism which has been observed in HTS vortex cores.[14–18] At the same time, there exist only very preliminary results of experimental and theoretical investigations of proximity and Josephson effects through various types of antiferromagnetic interfaces.[19–25] Below we study theoretically interfaces between itinerant antiferromagnets and normal metals or superconductors. Itinerant antiferromagnets, such as chromium and its alloys,[20,26,27] are metals above the Néel temperature. In the antiferromagnetic phase, however, an energy gap in the quasiparticle spectrum arises either on the whole Fermi surface or on parts of it. Similar properties are also manifested in Mott antiferromagnets, in particular undoped cuprates. Since they possess strong correlations due to large on-site Coulomb repulsion U, the mean-field approach of the present paper cannot be applied quantitatively to Mott systems, whereas it applies well to itinerant antiferromagnets with comparatively small U. We expect, however, that our main conclusions regarding AF/S and AF/N interfaces can be qualitatively applied also to interfaces with Mott antiferromagnets because they are based largely on symmetry properties and general characteristics of antiferromagnets, such as the doubling of period, nesting conditions and the wave vector of the antiferromagnetic pattern. In itinerant antiferromagnets, the energy gap in the quasiparticle spectrum is determined by the antiferromagnetic order parameter, i.e., the sublattice electronic magnetization m. This applies both to commensurate antiferromagnetic phases and to phases with spin-density waves,[28] and is reminiscent of the situation in superconductors, where the energy gap is determined by the superconducting order parameter Δ.

Recently, it has been demonstrated theoretically that a spin-dependent channel of quasiparticle reflection, the so-called Q reflection, takes place at interfaces between itinerant antiferromagnets and normal metals or superconductors.[25] Parallel to the interface, the momentum component of low-energy normal-metal quasiparticles changes by a wave vector $\boldsymbol{Q}_{\parallel}$ in a Q reflection event, where $\boldsymbol{Q}$ is the wave vector of the antiferromagnetic pattern. Assuming small Fermi velocity mismatches and taking into account the nesting condition $E_F(\boldsymbol{p}+\boldsymbol{Q})=-E_F(\boldsymbol{p})$ in itinerant antiferromagnets, one can see that a normal-metal quasiparticle changes its total momentum by $\boldsymbol{Q}$ and the respective velocity changes its sign in a Q reflection event. Hence, normal-metal quasiparticles with energies less than or comparable to the antiferromagnetic gap

 ©2005 The American Physical Society

experience spin-dependent retroreflection at antiferromagnet-normal metal (AF/*N*) transparent interfaces. Furthermore, *Q* reflection processes generate quasiparticle bound states below the AF gap in AF/*N*/AF junctions, analogously to the case of subgap states in SC/*N*/SC systems formed by the Andreev reflection. The AF/*N*/AF bound states arise from a coherent superposition of electrons with momenta $\boldsymbol{k}$ and $\boldsymbol{k}+\boldsymbol{Q}$ and almost opposite velocities. Subgap states arise also at AF/SC interfaces as a combined effect of Andreev and *Q* reflections. Among a variety of subgap states, low-energy states with energies $E_B \ll \min\{m,\Delta\}$ are of special interest since they can result in low-temperature anomalies in the Josephson critical current, as well as low-bias anomalies in the conductance. Low-energy quasiparticle interface states were also predicted to occur on antiferromagnetic–*s*-wave superconductor (AF/sSC) interfaces in the absence of specular reflection, when one can disregard effects of interface potential barriers and Fermi velocity mismatches. For an sSC/AF/sSC junction, these bound states are split due to a finite width of the AF interlayer and carry the supercurrent. At AF/dSC (*d*-wave superconductor) interfaces, low-energy bound states $E_B \ll \min\{m,\Delta\}$ do not exist, at least if the order parameters are small compared with the hopping matrix element ($\Delta, m \ll t$). This is contrary to the case of a (110) surface of a dSC confined with an impenetrable potential wall where zero-energy surface Andreev states are formed.[29–31]

Below, we extend the study of effects of *Q* reflection processes based on self-consistent solutions of the Bogoliubov–de Gennes (BdG) equations. This goes beyond the framework of our earlier work.[25] In general, we find excellent agreement with the results by Bobkova *et al.*[25] At the same time, the more general approach of the present paper allows us to study several important problems. In particular, we discuss the effects of interface potentials on the dispersive quasiparticle interface states and the local density of states (LDOS). In the presence of potential barriers and Fermi velocity mismatches, there exists an interplay of specular and *Q* reflections. We demonstrate that potential barriers on interfaces between AF and either sSC or dSC can result in additional extrema in dispersive quasiparticle spectra and associated peaks in the LDOS. We also find additional interface quasiparticle states with subgap energies near the edge of the continuum, which arise due to self-consistent suppression of the order parameters near the interface. By studying effects of interface pair breaking at AF/SC interfaces, we find that for the (110) orientation the self-consistent suppression of both antiferromagnetic and superconducting order parameters near the interface is accompanied by even-odd spatial oscillations. We show that discrete quasiparticle dispersive levels in AF-*N*-AF systems strongly depend on the relative orientation of the magnetizations in the two antiferromagnets. Effects of the misorientation angle turn out to be analogous to the influence of the phase difference on the discrete quasiparticle spectrum in SC-*N*-SC systems.

The paper is organized as follows. In Section II, we introduce the microscopic model used to study various interfaces with antiferromagnets, the BdG equations with a mean-field treatment of both magnetism and superconductivity general enough to study both *s*- and *d*-wave pairing symmetry, as well as various interface potentials. In Sec. III, we sketch the derivation of the associated quasiclassical (Andreev) equations complemented with boundary conditions by assuming slow spatial variations of both order parameters within each magnetic sublattice. In Sec. IV, we study quasiparticle states at (100) and (110) interfaces of both *s*- and *d*-wave superconductors with antiferromagnets, and compare the results of numerical evaluations of the BdG equations with the predictions of the quasiclassical theory. We end Sec. IV by showing how the bound state energies can be obtained within a transfer matrix formalism. In Sec. V we study the AF/*N*/AF junction, and discuss a "spin-π" configuration where the relative phase of the staggered magnetization on both sides of the junction can tune the energy of the interface bound states. Conclusions and perspectives for future work are presented in Sec. VI.

II. MODEL

For studying the electronic structure of interfaces between antiferromagnets and superconductors or normal metals, we consider the following two-dimensional (2D) mean-field Hamiltonian on a square lattice

$$\hat{H} = -t\sum_{\langle ij\rangle\sigma}\hat{c}^{\dagger}_{i\sigma}\hat{c}_{j\sigma} + \sum_{\langle ij\rangle}(\Delta_{ij}\hat{c}^{\dagger}_{i\uparrow}\hat{c}^{\dagger}_{j\downarrow} + \text{H.c.}) - \sum_{i\sigma}(\mu - h_i)\hat{n}_{i\sigma} + \sum_{i} m_i(\hat{n}_{i\uparrow} - \hat{n}_{i\downarrow}). \tag{1}$$

Here, Δ_{ij} and m_i denote the superconducting and magnetic order parameters, respectively. $\hat{c}^{\dagger}_{i\sigma}$ creates an electron of spin σ on the site i, t denotes the nearest-neighbor hopping integral, μ is the filling factor, h_i models possible interface potentials, and $\hat{n}_{i\sigma}=\hat{c}^{\dagger}_{i\sigma}\hat{c}_{i\sigma}$ is the particle number operator on site i. We will study self-consistently only singlet *s*-wave or *d*-wave superconducting pairings defined as $\Delta_{ij} = -(V_i/2)\langle \hat{c}_{i\downarrow}\hat{c}_{j\uparrow} - \hat{c}_{i\uparrow}\hat{c}_{j\downarrow}\rangle$. For *s*-wave pairing, one should set $i=j$, whereas the *d*-wave order parameter Δ_{ij} connects nearest neighbor sites. The self-consistent magnetic order parameter is represented as $m_i=(U_i/2)[\langle \hat{n}_{i\uparrow}\rangle - \langle \hat{n}_{i\downarrow}\rangle]$. In the bulk of the antiferromagnet and in the absence of any perturbations, the staggered magnetic order parameter takes the form $m_j = (-1)^{j_a+j_b}m = \exp(i\boldsymbol{Q}\boldsymbol{j})m$. For a square lattice with the crystal coordinate axes a and b, the antiferromagnetic wave vector is $\boldsymbol{Q}=(\pi/a,\pi/a)$. Within the framework of a generic Hubbard-type model, the staggered antiferromagnetic gapped state is stable only at or near half filling. For this reason we assume below vanishing or small μ.

We choose a coordinate system where x and y describe coordinates perpendicular and parallel to the interface, respectively. For a (100) interface the x and y axes coincide with the crystal axes a and b. Then the normal-state electron band is given by

$$\xi(\boldsymbol{k}) = -2t(\cos k_a + \cos k_b) - \mu, \tag{2}$$

and the respective Brillouin zone is spanned by $k_{a,b} \in [-\pi,\pi]$, with the momenta given in units of a^{-1}. For a (110) interface we have instead

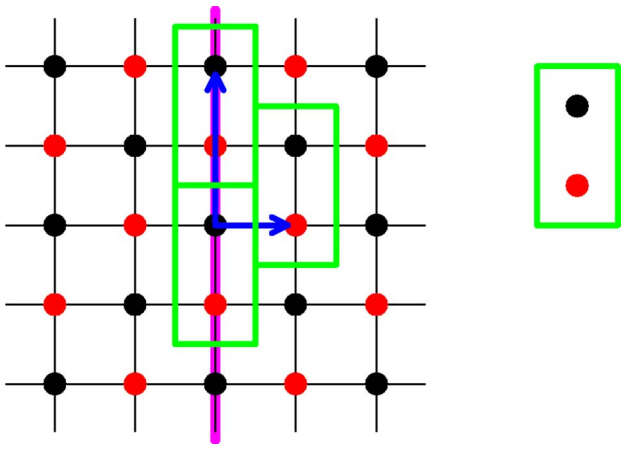

FIG. 1. (Color online) (100) interface, showing the corresponding unit cells with two atoms and basis vectors $\vec{e}_1$, $\vec{e}_2$ of the magnetic lattice.

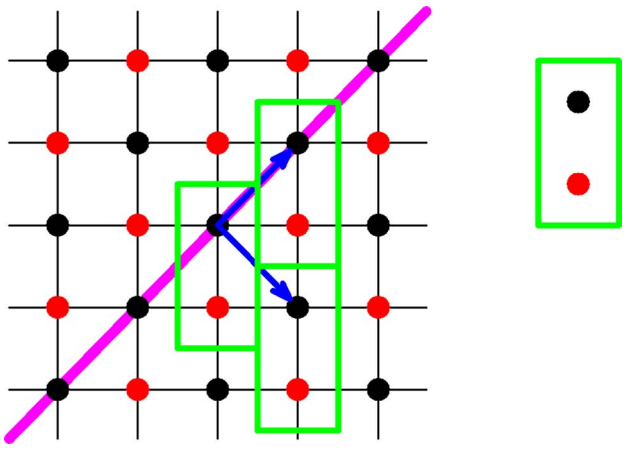

FIG. 2. (Color online) (110) interface, showing the corresponding unit cells and basis vectors.

$$\xi(\boldsymbol{k}) = -4t\cos(k_x/\sqrt{2})\cos(k_y/\sqrt{2}) - \mu, \tag{3}$$

with $k_x \in [-\sqrt{2}\pi, \sqrt{2}\pi]$, and $k_y \in [-\pi/\sqrt{2}, \pi/\sqrt{2}]$, on account of the periodic conditions along the crystal surface.

The Hamiltonian (1) is quadratic in the Fermi fields and can be diagonalized with Bogoliubov transformations, $\hat{c}^{\dagger}_{i\sigma} = \Sigma_n[u^{*}_{n\sigma}(i)\hat{\gamma}^{\dagger}_{n\sigma} + \sigma v_{n\sigma}(i)\hat{\gamma}_{n\bar{\sigma}}]$. The corresponding Bogoliubov–de Gennes equations take the form

$$\sum_j \begin{pmatrix} \mathcal{K}^{+}_{ij,\sigma} & \mathcal{D}_{ij,\sigma} \\ \mathcal{D}^{*}_{ij,\sigma} & -\mathcal{K}^{-}_{ij,\sigma} \end{pmatrix} \begin{pmatrix} u_{n\sigma}(j) \\ v_{n\bar{\sigma}}(j) \end{pmatrix} = E_{n\sigma} \begin{pmatrix} u_{n\sigma}(i) \\ v_{n\bar{\sigma}}(i) \end{pmatrix}. \tag{4}$$

Here $\mathcal{K}^{\pm}_{ij,\sigma} = -t\delta_{\langle ij\rangle} + (h_i - \mu)\delta_{ij} \pm \sigma m_i \delta_{ij}$, where $\sigma = \pm 1$ for up and down spin, δ_{ij} and $\delta_{\langle ij\rangle}$ are the Kronecker delta symbols connecting on-site and nearest neighbor sites, respectively. The off-diagonal block $\mathcal{D}_{ij,\sigma}$ connects the nearest neighbor links $\mathcal{D}_{ij,\sigma} = -\Delta_{ij}\delta_{\langle ij\rangle}$ with minus (plus) signs on the $a(b)$ links for the $d_{x^2-y^2}$-wave pairing symmetry, or on-site coupling $\mathcal{D}_{ij,\sigma} = -\Delta_i \delta_{ij}$ for conventional s-wave pairing. We note that a modified Bogoliubov transformation $\hat{c}^{\dagger}_{i\sigma} = \Sigma_n[u^{*}_{n\sigma}(i)\hat{\gamma}^{\dagger}_{n\sigma} + v_{n\sigma}(i)\hat{\gamma}_{n\bar{\sigma}}]$, implemented in Ref. 25, led to modified amplitudes $v_{n\sigma}(i)$: $v_{n\sigma}(i) \to \sigma v_{n\sigma}(i)$. The corresponding basic equations for these modified amplitudes coincide with those in the present paper [in particular, see Eqs. (4), (6)–(9), (13), and (14)] after redefining the off-diagonal blocks $\mathcal{D}_{ij,\sigma} \to -\sigma\mathcal{D}_{ij,\sigma}$, or, equivalently, $\Delta_{ij} \to -\sigma\Delta_{ij}$, $\Delta_i \to -\sigma\Delta_i$.

Crystal periodicity along the interface makes it convenient to Fourier transform the BdG equations along the y axis and introduce a wave vector component k_y, as usual.[32] In the presence of antiferromagnetic ordering, this should be done by taking into account magnetic crystal symmetry along the boundary. In particular, the magnetic order parameter m_j oscillates rapidly along the (100) interface and results in a doubling of the period along the y axis. In general, a modified magnetic period along the boundary arises for all interface orientations except for a (110) interface. We will take into account the magnetic crystal symmetry by introducing a unit cell which contains two neighboring atoms which belong to different magnetic sublattices A and B. Unit cells chosen below for the (100) and (110) interface are shown in Figs. 1 and 2, respectively.

On account of the magnetic crystal symmetry, the Fourier transformation is taken to be of the form

$$\begin{pmatrix} u^{A(B)}_{j,\sigma} \\ v^{A(B)}_{j,\bar{\sigma}} \end{pmatrix} = \frac{d_y}{2\pi} \int_{-\pi/d_y}^{\pi/d_y} dk_y e^{ik_y d_y j_y} \begin{pmatrix} u^{A(B)}_{j_x,\sigma}(k_y) \\ v^{A(B)}_{j_x,\bar{\sigma}}(k_y) \end{pmatrix}. \tag{5}$$

Here k_y is measured in units of a^{-1} and $d_y = 2, \sqrt{2}$ for (100), and (110) interfaces, respectively. The transformation is identical for atoms of sublattices A and B in the same unit cell $\boldsymbol{j}$. The vector $\boldsymbol{j} = (j_x, j_y)$ denotes cell coordinates, where $j_{x(y)}$ is the $x(y)$ coordinate of the cell measured in units of the appropriate basis vectors. For definiteness, we identify cell positions with positions of the associated site A.

Let vector $\boldsymbol{i}$ denote the location of a nearest neighbor site for site $A(B)$ in the same unit cell. Then, the positions of all nearest neighbors are described in the case of a (100) interface in terms of the basis vectors shown in Fig. 1 as $\langle \boldsymbol{i} + \boldsymbol{e}_1 \pm (\boldsymbol{e}_2/2), \boldsymbol{i} - \boldsymbol{e}_1 \pm (\boldsymbol{e}_2/2), \boldsymbol{i} \pm \boldsymbol{e}_2, \boldsymbol{i}\rangle$. Taking this into account when performing the Fourier transformation (5) in Eqs. (4), we obtain the following one-dimensional Bogoliubov–de Gennes equations for the (100) case:

$$-\mu u^{A(B)}_{j,\sigma}(k_y) - te^{\pm ik_y}[u^{B(A)}_{j+1,\sigma}(k_y) + u^{B(A)}_{j-1,\sigma}(k_y) + 2\cos k_y u^{B(A)}_{j,\sigma}(k_y)] + \sigma m^{A(B)}_j u^{A(B)}_{j,\sigma}(k_y) - \Delta^{A(B)}_{s,j} v^{A(B)}_{j\bar{\sigma}}(k_y) - e^{\pm ik_y}[\Delta^{A(B),a}_{d,jj+1} v^{B(A)}_{j+1,\bar{\sigma}}(k_y) + \Delta^{A(B),a}_{d,jj-1} v^{B(A)}_{j-1,\bar{\sigma}}(k_y) + 2\cos k_y \Delta^{A(B),b}_{d,jj} v^{B(A)}_{j,\bar{\sigma}}(k_y)] = E u^{A(B)}_{j,\sigma}(k_y), \tag{6}$$

$$\mu v^{A(B)}_{j,\bar{\sigma}}(k_y) + te^{\pm ik_y}[v^{B(A)}_{j+1,\bar{\sigma}}(k_y) + v^{B(A)}_{j-1,\bar{\sigma}}(k_y) + 2\cos k_y v^{B(A)}_{j,\bar{\sigma}}(k_y)] + \sigma m^{A(B)}_j v^{A(B)}_{j,\bar{\sigma}}(k_y) - \Delta^{A(B)^*}_{s,j} u^{A(B)}_{j,\sigma}(k_y) - e^{\pm ik_y}[\Delta^{A(B),a^*}_{d,jj+1} u^{B(A)}_{j+1,\sigma}(k_y) + \Delta^{A(B),a^*}_{d,jj-1} u^{B(A)}_{j-1,\sigma}(k_y) + 2\cos k_y \Delta^{A(B),b^*}_{d,jj} u^{B(A)}_{j,\sigma}(k_y)] = E v^{A(B)}_{j,\bar{\sigma}}(k_y). \quad (7)$$

Here, j denotes only the x coordinate of a cell. The factors $\exp(\pm ik_y)$ arise in the nonlocal terms in Eqs. (6) and (7) since for the (100) interface orientation, in accordance with the definitions above, the y coordinate of the site B is always less by a than the coordinate of site A in the same cell.

For the (110) orientation, however, the y coordinate of the site B is less by $a/\sqrt{2}$ than the y coordinate of site A in the same cell. Furthermore, if the vector $\boldsymbol{i}$ denotes the location of a nearest neighbor site for site $A(B)$ in the same unit cell, the positions of all nearest neighbors in the case of the (110) interface are described in terms of basis vectors shown in Fig. 2 as $\langle \boldsymbol{i} \mp \boldsymbol{e}_1, \boldsymbol{i} \pm \boldsymbol{e}_2, \boldsymbol{i}, \boldsymbol{i} \mp \boldsymbol{e}_1 \pm \boldsymbol{e}_2 \rangle$. Thus, for the (110) interface orientation we obtain the following one-dimensional BdG equations:

$$-\mu u^{A(B)}_{j,\sigma}(k_y) - 2t\cos\frac{k_y}{\sqrt{2}} e^{\pm ik_y/\sqrt{2}}[u^{B(A)}_{j,\sigma}(k_y) + u^{B(A)}_{j\mp 1,\sigma}(k_y)] + \sigma m^{A(B)}_j u^{A(B)}_{j,\sigma}(k_y) - \Delta^{A(B)}_{s,j} v^{A(B)}_{j,\bar{\sigma}}(k_y) - \{[\Delta^{A(B),a}_{d,jj} e^{\pm\sqrt{2}ik_y} + \Delta^{A(B),b}_{d,jj}] v^{B(A)}_{j,\bar{\sigma}}(k_y) + [\Delta^{A(B),b}_{d,jj\mp 1} e^{\pm\sqrt{2}ik_y} + \Delta^{A(B),a}_{d,jj\mp 1}] v^{B(A)}_{j\mp 1,\bar{\sigma}}(k_y)\} = E u^{A(B)}_{j,\sigma}(k_y), \quad (8)$$

$$\mu v^{A(B)}_{j,\bar{\sigma}}(k_y) + 2t\cos\frac{k_y}{\sqrt{2}} e^{\pm ik_y/\sqrt{2}}[v^{B(A)}_{j,\bar{\sigma}}(k_y) + v^{B(A)}_{j\mp 1,\bar{\sigma}}(k_y)] + \sigma m^{A(B)}_j v^{A(B)}_{j,\bar{\sigma}}(k_y) - \Delta^{A(B)^*}_{s,j} u^{A(B)}_{j,\sigma}(k_y) - [(\Delta^{A(B),a^*}_{d,jj} e^{\pm\sqrt{2}ik_y} + \Delta^{A(B),b^*}_{d,jj}) u^{B(A)}_{j,\sigma}(k_y) + (\Delta^{A(B),b^*}_{d,jj\mp 1} e^{\pm\sqrt{2}ik_y} + \Delta^{A(B),a^*}_{d,jj\mp 1}) u^{B(A)}_{j\mp 1,\sigma}(k_y)] = E v^{A(B)}_{j,\bar{\sigma}}(k_y). \quad (9)$$

The singlet superconducting order parameters entering Eqs. (6)–(9) are defined as $\Delta^{A(B)}_{ij} = -(V_i/2)\langle \hat{c}^{A(B)}_{i\downarrow} \hat{c}^{B(A)}_{j\uparrow} - \hat{c}^{A(B)}_{i\uparrow} \hat{c}^{B(A)}_{j\downarrow} \rangle$. The magnetic order parameter is $m^{A(B)}_i = (U_i/2) \times [\langle \hat{n}^{A(B)}_{i\uparrow} \rangle - \langle \hat{n}^{A(B)}_{i\downarrow} \rangle]$. For the study of proximity effects, it is convenient to introduce the magnetization M_i and the pairing amplitude F_{ij}, which are related to m_i and Δ_{ij} by $m_i = U_i M_i$ and $\Delta_{ij} = -V_i F_{ij}$, respectively.

The self-consistency equations in the sublattice representation take the form

$$n^{A(B)}_{i\sigma} = \sum_{n,k_y} [|u^{A(B)}_{n,i_x,\sigma}(k_y)|^2 f(E_{n,k_y,\sigma}) + |v^{A(B)}_{n,i_x,\sigma}(k_y)|^2 f(-E_{n,k_y,\sigma})], \quad (10)$$

$$\Delta^{A(B)}_{ij} = -\frac{V_i}{2} \sum_{n,k_y,\sigma} [u^{A(B)}_{n,i_x,\sigma}(k_y) v^{B(A)^*}_{n,j_x,\bar{\sigma}}(k_y) e^{ik_y d_y (i_y - j_y)} f(-E_{n,k_y,\sigma}) - u^{B(A)}_{n,j_x,\sigma}(k_y) v^{A(B)^*}_{n,i_x,\bar{\sigma}}(k_y) e^{-ik_y d_y (i_y - j_y)} f(E_{n,k_y,\sigma})]. \quad (11)$$

The sum is taken over eigenstates of Eqs. (6)–(9), which depend on k_y, σ, and possibly an additional set of quantum numbers n. Equation (11) applies to the d-wave case, whereas for the s-wave superconductor with on-site pairing one should put in Eq. (11) Δ^{α}_{ii} with amplitudes $u^{\alpha}_{n,i_x,\sigma}(k_y)$, $v^{\alpha}_{n,i_x,\bar{\sigma}}(k_y)$ taken for one sublattice $\alpha = A, B$. As usual, $f(E) = [1 + \exp(E/T)]^{-1}$ denotes the Fermi distribution function at temperature T.

Obviously, any bond between nearest neighbors connects two sites from different sublattices. The notation Δ^{A}_{ij} (Δ^{B}_{ij}) means that the order parameter is taken on the bond which connects a site of sublattice $A(B)$ within the unit cell i with a nearest neighbor site [of sublattice $B(A)$] in the unit cell j. All order parameters are presumed to be identical on links (or sites) which can be obtained from each other by magnetic translations along the interface or interlayer. For this reason, it is sufficient to consider i and j in the notation $\Delta^{A(B)}_{ij}$ as containing only x components, if one indicates in addition the type of link (a or b).

III. ANDREEV EQUATIONS AND $\mathcal{S}$ MATRICES

We will base our numerical calculations on the one-dimensional Bogoliubov–de Gennes equations formulated above, as well as on the corresponding self-consistency equations. For an analytical study of superconducting interfaces and junctions involving itinerant antiferromagnets, we present in this section the quasiclassical approach developed in Ref. 25. As is well known, the quasiclassical theory describes physical quantities which vary slowly in space compared to the atomic scale and assumes characteristic energies to be much less than the Fermi energy E_F. We consider below two types of superconductor-antiferromagnet hybrid sys-

tems to which the quasiclassical approach applies to a different extent.

The first type of system satisfies the conditions $|\Delta| \ll E_F$, $|m| \ll E_F$. The latter inequality guarantees that the antiferromagnetic order parameter m, as a rule, varies slowly within each separate sublattice A and B. Hence, one can use quasiclassical equations both for superconducting and antiferromagnetic phases and match them at the interface if they are formulated separately for each sublattice. Sublattice equations are coupled with each other via nonlocal terms which contain, for example, hopping matrix elements or d-wave superconducting order parameter fields. In total, this gives us twice the usual number of coupled quasiclassical equations. Another possible formulation of the quasiclassical approach to the first type of superconductor itinerant antiferromagnet hybrid system is not based on the sublattice representation. Instead, one can formulate equations for quasiparticle trajectories, taking into account that the rapidly oscillating antiferromagnetic order parameter $m_j=(-1)^{j_a+j_b}m=\exp(i\boldsymbol{Q}\boldsymbol{j})m$ couples equations for two trajectories, one for a quasiparticle momentum $\boldsymbol{k}_F$ and the other for $(\boldsymbol{k}_F+\boldsymbol{Q})$. The approach based on this $(\boldsymbol{k}_F,\boldsymbol{k}_F+\boldsymbol{Q})$ representation results also in twice the number of quasiclassical equations. There are no further coupled trajectories, since $2\boldsymbol{Q}$ is assumed to be the reciprocal vector of the nonmagnetic crystal due to the nesting condition.

In the second type of hybrid superconductor-antiferromagnet system, only the superconducting order parameter satisfies the condition $|\Delta| \ll E_F$ and can be safely described with the quasiclassical equations. The antiferromagnetic order parameter is taken as sufficiently large $\Delta \ll |m| \lesssim E_F$ (one could also assume $m \gtrsim E_F$ within the framework of the approach, if this were relevant). Then the effect of the antiferromagnet on the superconductor can be taken into account entirely via modified boundary conditions, which complement quasiclassical equations at abrupt superconductor-antiferromagnetic interfaces.

A. Andreev equations in the sublattice representation

We begin with the derivation of Andreev equations in the sublattice representation. Assume for this purpose that the solution of the BdG equations (6)–(9) can be represented as the following product of rapidly oscillating exponents and a slowly varying Andreev amplitude:

$$\begin{pmatrix} u^A_{j\sigma} \\ u^B_{j\sigma} \\ v^A_{j\bar{\sigma}} \\ v^B_{j\bar{\sigma}} \end{pmatrix} = \exp\left(i\frac{\boldsymbol{k}_F\hat{\boldsymbol{b}}}{2}\hat{\gamma}_3 \right) \begin{pmatrix} \tilde{u}^A_{j\sigma} \\ \tilde{u}^B_{j\sigma} \\ \tilde{v}^A_{j\bar{\sigma}} \\ \tilde{v}^B_{j\bar{\sigma}} \end{pmatrix} \exp(ik_{F,x}d_x j). \qquad (12)$$

Here, $k_{F,x}$ is the x component of the quasiparticle momentum on the Fermi surface, measured in units of a^{-1}. The quantity $k_{F,x}$ can be considered a function of k_y. The Pauli matrix $\hat{\gamma}_3$ operates in (AB) sublattice space, $d_x=1$ for (100) interface and $d_x=\sqrt{2}$ for the (110) case. Introducing the unit vector $\hat{\boldsymbol{b}}$ along the crystal b axis permits us to define the Andreev amplitudes in Eq. (12) in a unified form which applies to all interface orientations.

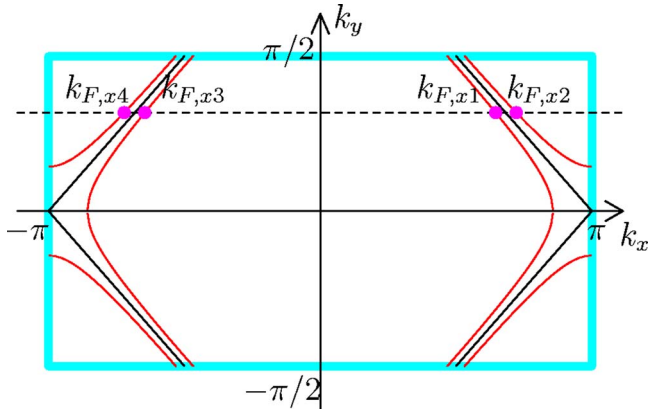

FIG. 3. (Color online) The Brillouin zone adapted to the (100) interface and the Fermi surfaces for small and vanishing μ.

As mentioned above, the parameter μ is considered throughout the paper to be small $\mu \ll E_F$, since the antiferromagnetic phase is stable only close to half filling. For this reason, one can additionally include effects of small deviations from half filling in the quasiclassical approximation. Taking this into account, we define a small parameter of the quasiclassical expansion as $\alpha=\max(|m|,|\Delta|,|\mu|)a/|v_{F,x}| \ll 1$. Here $v_{F,x}$ is the x component of the Fermi velocity in the normal metal state at half filling. The quasiclassical approach works only for those k_y for which $v_{F,x}$ is not too small and does not break the condition $\alpha \ll 1$. We expand all properties associated with the Fermi surface in powers of the small parameter $(\mu a/|v_{F,x}|) \ll 1$. This concerns, in particular, $k_{F,x}$, which enters the exponential factor in Eq. (12). The surface-adapted Brillouin zone and respective Fermi surface for small and vanishing μ are shown in Figs. 3 and 4 for the (100) and (110) interface orientations, respectively.

For the (100) orientation, the normal-state electron band is described as $\xi^{\pm}(\boldsymbol{k})=\mp 2t(\cos k_x+\cos k_y)-\mu$, and the Brillouin zone in the case of two atoms in the unit cell (see Fig. 1) is spanned by $k_x \in [-\pi,\pi]$, $k_y \in [-\pi/2,\pi/2]$. For the half-filled band $k_{F,x}=\pm(\pi-|k_y|)$ and $v^{\pm}_{F,x}=\pm 2ta \sin k_{F,x}$. As is seen in Fig. 3, four possible values of $k_{F,x}$, which occur for a given k_y at $\mu \neq 0$, merge into two values at $\mu=0$.

For the (110) interface, we have in the sublattice representation $\xi^{\pm}(\boldsymbol{k})=\mp 4t\cos(k_x/\sqrt{2})\cos(k_y/\sqrt{2})-\mu$ and $k_{x,y} \in [-\pi/\sqrt{2},\pi/\sqrt{2}]$. If $\mu>0$, only the Fermi surface $\xi^{-}(\boldsymbol{k})=0$ exists in the first Brillouin zone, whereas for $\mu<0$ the Fermi surface is determined from $\xi^{+}(\boldsymbol{k})=0$. At $\mu=0$ both Fermi

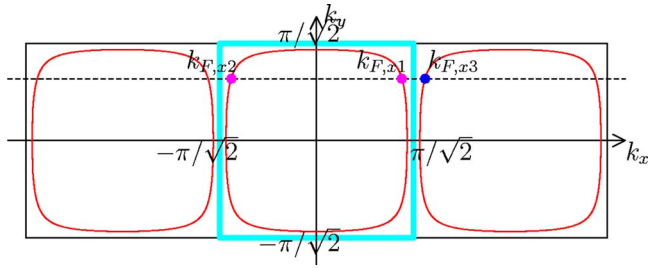

FIG. 4. (Color online) The Brillouin zone adapted to (110) interface and the Fermi surfaces for small and vanishing μ.

surfaces coincide with the edges of the first Brillouin zone. As seen in Fig. 4, two different values of $k_{F,x}$, which occur within the first Brillouin zone for a given k_y, touch the edges of the zone $k_{F,x}=\pm\pi/\sqrt{2}$ in the case of half filling and hence, become equivalent at $\mu=0$. Since the Fermi velocities v_{F,x_1} and v_{F,x_3} have opposite signs, for the half-filled band $v^{\pm}_{F,x}(\boldsymbol{k}_F)=\pm 2\sqrt{2}ta\cos(k_y/\sqrt{2})$, where two signs of $v_{F,x}(\boldsymbol{k}_F)$ at the same $\boldsymbol{k}_F$ correspond to two degenerate parts of the Fermi surface.

To obtain the Andreev equations for the (100) orientation, we substitute the ansatz (12) into Eqs. (6) and (7), separately for each of the two values $k_{F,x}=\pm(\pi-k_y)$, and disregard terms $\lesssim\alpha^2$. For the (110) interface one should proceed analogously, using in Eqs. (8) and (9) the ansatz (12) with $k_{F,x}=\pi/\sqrt{2}$. We note that $|\tilde{u}^{B(A)}_{j\pm1,\sigma}-\tilde{u}^{B(A)}_{j,\sigma}|\lesssim\alpha|\tilde{u}^{B(A)}_{j,\sigma}|$, $|\tilde{u}^{B(A)}_{j+1,\sigma}+\tilde{u}^{B(A)}_{j-1,\sigma}-2\tilde{u}^{B(A)}_{j,\sigma}|\lesssim\alpha^2|\tilde{u}^{B(A)}_{j,\sigma}|$. Neglecting terms of the order of α^2, one gets with the required accuracy $\tilde{u}^{\nu}_{j+1}-\tilde{u}^{\nu}_{j}=\tilde{u}^{\nu}_{j}-\tilde{u}^{\nu}_{j-1}=(\tilde{u}^{\nu}_{j+1}-\tilde{u}^{\nu}_{j-1})/2=d_x\partial\tilde{u}^{\nu}_{j}/\partial x_j$.

Using the outlined procedure, we obtain the following Andreev equations in the sublattice representation:

$$-\mu\tilde{u}^{A(B)}_{j,\sigma}-iv^{+}_{F,x}\frac{\partial\tilde{u}^{B(A)}_{j,\sigma}}{\partial x_j}+\sigma m^{A(B)}_{j}\tilde{u}^{A(B)}_{j,\sigma}-\Delta^{A(B)}_{s,j}\tilde{v}^{A(B)}_{j,\bar{\sigma}}-\Delta^{A(B)}_{d,j}(k_{F,x},k_y)\tilde{v}^{B(A)}_{j,\bar{\sigma}}=E_\sigma\tilde{u}^{A(B)}_{j,\sigma},\tag{13}$$

$$\mu\tilde{v}^{A(B)}_{j,\bar{\sigma}}+iv^{+}_{F,x}\frac{\partial\tilde{v}^{B(A)}_{j,\bar{\sigma}}}{\partial x_j}+\sigma m^{A(B)}_{j}\tilde{v}^{A(B)}_{j,\bar{\sigma}}-\Delta^{A(B)^*}_{s,j}\tilde{u}^{A(B)}_{j,\sigma}-\Delta^{A(B)^*}_{d,j}(k_{F,x},k_y)\tilde{u}^{B(A)}_{j,\sigma}=E_\sigma\tilde{v}^{A(B)}_{j,\bar{\sigma}}.\tag{14}$$

These equations take a unified form, which applies to any interface orientation. For the (100) orientation $\Delta^{A(B)}_{d,j}(k_{F,x},k_y)=2\Delta^{A(B)}_{d,j}(\cos k_{F,x}-\cos k_y)$. The on-site d-wave order parameter $\Delta^{A(B)}_{d,j}$, slowly varying on the atomic scale with coordinate j along x axis, is defined in the coordinate space by the four surrounding links. With standard site coordinates $\boldsymbol{i}=(i_x,i_y)$ one can write $\Delta_{d,i}=\frac{1}{4}(\Delta_{d,ii+a}+\Delta_{d,ii-a}-\Delta_{d,ii+b}-\Delta_{d,ii-b})$. For the (110) orientation we have $\Delta^{A(B)}_{d,j}(k_{F,x},k_y)=-4\Delta^{A(B)}_{d,j}\sin(k_{F,x}/\sqrt{2})\sin(k_y/\sqrt{2})$ with $k_{F,x}=\pi/\sqrt{2}$.

As one can see from the derivation of Eqs. (13) and (14), they apply to various cases when the sublattice magnetic and/or superconducting order parameters vary slowly in space, satisfying standard quasiclassical conditions. For instance, no particular relation between the sublattice magnetizations m^A_j and m^B_j is implied yet. For both interface orientations, the Fermi velocity $v^{+}_{F,x}(\boldsymbol{k}_F)$ is positive for $k_{F,x}>0$ within the Brillouin zone in the sublattice representation. However, the associated solutions of Eqs. (13) and (14) can describe, in general, both incoming and outgoing quasiparticles on either side of the interface. This is seen from the expression for the density of a quasiparticle probability current $\boldsymbol{j}_P$, which can be found from the BdG equations in much the same standard way known in the case of the Schrödinger equation. The probability current density along the x axis, carried by the solution with quantum numbers (n,σ,k_y), can be written in the (100) case as

$$j_{P,x}=\frac{v^{+}_{F,x}}{2a}\sum_{\alpha=\pm,\nu}[\alpha(\tilde{u}^{j,\nu^*}_{n,\sigma,\alpha}\tilde{u}^{j,\bar{\nu}}_{n,\sigma,\alpha}-\tilde{v}^{j,\nu}_{n,\bar{\sigma},\alpha}\tilde{v}^{j,\bar{\nu}^*}_{n,\bar{\sigma},\alpha})].\tag{15}$$

Here, the sum is taken over sublattice index $\nu=A,B$, as well as over the two parts of the Fermi surface $\alpha=\pm1$.

For the (110) orientation we find

$$j_{P,x}=\frac{v^{+}_{F,x}}{2a}\sum_{\nu}[(\tilde{u}^{j,\nu^*}_{n,\sigma}\tilde{u}^{j,\bar{\nu}}_{n,\sigma}-\tilde{v}^{j,\nu}_{n,\bar{\sigma}}\tilde{v}^{j,\bar{\nu}^*}_{n,\bar{\sigma}})].\tag{16}$$

As usual, the components u and v of the Andreev amplitudes with the same wave vector have opposite contributions to the probability current.[33] Since the current is formed mainly by hopping between nearest neighbor sites, it is determined in the sublattice representation as a mixed product of A and B components of Andreev amplitudes for any interface orientation. Hence, the sign of $j_{P,x}$ depends not only on the crystal wave vector $\mathbf{k}_F$, but also on the *relative* signs of the A and B components of the Andreev amplitudes.

One can further transform Eqs. (13) and (14), which are formulated in the (AB)-sublattice representation with two atoms per unit cell into the representation with one atom per unit cell. Consider, for example, the (110) interface orientation. For one atom per unit cell, the Brillouin zone is spanned by $k_x\in[-\sqrt{2}\pi,\sqrt{2}\pi]$, $k_y\in[-\pi/\sqrt{2},\pi/\sqrt{2}]$ and $\xi(\boldsymbol{k})$ is given in Eq. (3), whereas in the case of two atoms per unit cell the Brillouin zone in the k_x direction is $k_x\in[-\pi/\sqrt{2},\pi/\sqrt{2}]$. Assuming $|k_{F,x}|\leq\pi/\sqrt{2}$, one can write the following relation between the quasiparticle amplitudes in the two representations [compare with Eq. (12)]:

$$\begin{pmatrix}\tilde{u}^{A}_{j}(\boldsymbol{k}_F)e^{i(k_y-k_{F,x})/2\sqrt{2}}\\ \tilde{u}^{B}_{j}(\boldsymbol{k}_F)e^{-i(k_y-k_{F,x})/2\sqrt{2}}\end{pmatrix}\times e^{ik_{F,x}\sqrt{2}j}=\begin{pmatrix}\tilde{u}_{2j}(\boldsymbol{k}_F)\\ \tilde{u}_{2j+1}(k_F)e^{-i(k_y-k_{F,x})/\sqrt{2}}\end{pmatrix}e^{i(k_{F,x}/\sqrt{2})2j}+\begin{pmatrix}\tilde{u}_{2j}(\boldsymbol{k}_F+\boldsymbol{Q})\\ -\tilde{u}_{2j+1}(\boldsymbol{k}_F+\boldsymbol{Q})e^{-i(k_y-k_{F,x})/\sqrt{2}}\end{pmatrix}e^{i(k_{F,x}/\sqrt{2})2j}.\tag{17}$$

Here, we have taken into account that if j is the x coordinate of a two-atom unit cell, then in the representation with one atom per unit cell, the site A has even x coordinate $2j$, whereas site B has the odd coordinate $2j+1$.

In the sublattice representation, the wave vector $\boldsymbol{Q}=(\pm\sqrt{2}\pi,0)$, which is the wave vector of the antiferromagnetic pattern that we will study below, is the reciprocal crystal vector. Thus, the wave vectors $\boldsymbol{k}_F$ and $\boldsymbol{k}_F+\boldsymbol{Q}$ are equivalent to each other in the approach with two atoms per unit cell. In the representation with one atom per unit cell, the wave vectors $\boldsymbol{k}_F$ and $\boldsymbol{k}_F+\boldsymbol{Q}$ are physically different. The quantity $\boldsymbol{k}_F+\boldsymbol{Q}$ in Eq. (17) is assumed to lie in the first Brillouin zone of the representation with one atom per unit cell, so that $\boldsymbol{Q}=(\pm\sqrt{2}\pi,0)$ should be taken there with a minus sign for $0<k_{F,x}\leq\pi/\sqrt{2}$ and with plus sign for $-\pi/\sqrt{2}\leq k_{F,x}\leq0$. Thus, it follows from Eq. (17) that

$$\begin{pmatrix} \tilde{u}_j^A(\boldsymbol{k}_F) \\ \tilde{u}_j^B(\boldsymbol{k}_F) \end{pmatrix} = \begin{pmatrix} \tilde{u}_{2j}(\boldsymbol{k}_F) + \tilde{u}_{2j}(\boldsymbol{k}_F + \boldsymbol{Q}) \\ \tilde{u}_{2j+1}(\boldsymbol{k}_F) - \tilde{u}_{2j+1}(\boldsymbol{k}_F + \boldsymbol{Q}) \end{pmatrix} e^{-i[(k_y - k_{F,x})/2\sqrt{2}]}. \tag{18}$$

For the (100) interface orientation, the Brillouin zone for the square lattice with one atom per unit cell is spanned by $k_{x,y} \in [-\sqrt{2}\pi, \sqrt{2}\pi]$ and $\xi(\boldsymbol{k})$ is given in Eq. (2), whereas for two atoms per unit cell, shown in Fig. 2, the Brillouin zone in the k_y direction is $k_y \in [-\pi/\sqrt{2}, \pi/\sqrt{2}]$. Assuming $|k_{F,y}| \leq \pi/\sqrt{2}$, we find the following relation between the quasiparticle amplitudes in the two representations:

$$\begin{pmatrix} \tilde{u}_j^A(k_y) \\ \tilde{u}_j^B(k_y) \end{pmatrix} = \frac{1}{2} e^{-ik_y/2} \begin{pmatrix} \tilde{u}_j(k_y) + \tilde{u}_j(k_y + Q_y) \\ \tilde{u}_j(k_y) - \tilde{u}_j(k_y + Q_y) \end{pmatrix}. \tag{19}$$

Here, the wave vector $\boldsymbol{Q} = (\pm\pi, \pm\pi)$ is the reciprocal crystal vector in the sublattice representation. The quantity $k_y + Q_y$ in Eq. (19) is assumed to lie in the first Brillouin zone of the representation with one atom per unit cell so that $Q_y = \pm\pi$ should be taken with a minus sign for $0 < k_{F,y} \leq \pi/\sqrt{2}$ and with a plus sign for $-\pi/\sqrt{2} \leq k_{F,y} \leq 0$.

Substituting Eq. (18) and (19) into Eqs. (13) and (14), we obtain the Andreev equations in the $(\boldsymbol{k}_F, \boldsymbol{k}_F + \boldsymbol{Q})$ representation. Since quasiparticle crystal momenta $\boldsymbol{k}_F$ and $\boldsymbol{k}_F + \boldsymbol{Q}$ both lie on the Fermi surfaces on either side of the interface, the Andreev equation in the $(\boldsymbol{k}_F, \boldsymbol{k}_F + \boldsymbol{Q})$ representation takes the comparatively simple form

$$\begin{aligned} \Bigg(& -iv_{F,x}(\boldsymbol{k}_F)\hat{\rho}_z\hat{\tau}_z\frac{\partial}{\partial x_j} - \mu\hat{\tau}_z + \sigma\frac{m_j^A + m_j^B}{2} + \sigma\frac{m_j^A - m_j^B}{2}\hat{\rho}_x \\ & - \Delta_{s,j}\frac{\hat{\tau}_+}{2} - \Delta_{s,j}^*\frac{\hat{\tau}_-}{2} - \Delta_{d,j}(\boldsymbol{k}_F)\frac{\hat{\tau}_+}{2}\hat{\rho}_z - \Delta_{d,j}^*(\boldsymbol{k}_F)\frac{\hat{\tau}_-}{2}\hat{\rho}_z \Bigg)\hat{\Psi}_{j\sigma} \\ & = E_\sigma \hat{\Psi}_{j\sigma}. \end{aligned} \tag{20}$$

Here, $\hat{\Psi}_{j\sigma} = (\tilde{u}_{j\sigma}(\boldsymbol{k}_F), \tilde{u}_{j\sigma}(\boldsymbol{k}_F + \boldsymbol{Q}), \tilde{v}_{j\bar{\sigma}}(\boldsymbol{k}_F), \tilde{v}_{j\bar{\sigma}}(\boldsymbol{k}_F + \boldsymbol{Q}))$. $\hat{\tau}_\alpha$ and $\hat{\rho}_\alpha$ denote the Pauli matrices in particle-hole and $\{\boldsymbol{k}_F, \boldsymbol{k}_F + \boldsymbol{Q}\}$ spaces. Equation (20) applies generally for any particular relation between m_j^A and m_j^B. For instance, it applies also to the study of weak ferromagnets ($m \ll \varepsilon_f$). In the case of antiferromagnetic ordering satisfying the condition $m_j^B = -m_j^A$, within the quasiclassical accuracy one can disregard in Eq. (20) the term containing $m_j^A + m_j^B$.

The only term which couples Andreev amplitudes with momenta $\boldsymbol{k}_F$ and $\boldsymbol{k}_F + \boldsymbol{Q}$ in Eq. (20) contains the difference between sublattice magnetizations $m_j^A - m_j^B$. This is natural, since a finite difference $m_j^A - m_j^B$ results in a doubling of the period in the system which we study. Equations (13), (14), and (20) apply also in the absence of period doubling, being equivalent in this case to the standard Andreev equations. If period doubling takes place only at the boundaries, the sublattice or $(\boldsymbol{k}_F, \boldsymbol{k}_F + \boldsymbol{Q})$ representations of the quasiclassical equations can be convenient for applying appropriate boundary conditions to the solutions.

B. Boundary conditions and the $\mathcal{S}$ matrix in $(\boldsymbol{k}_F, \boldsymbol{k}_F + \boldsymbol{Q})$ representation

The assumption of slowly varying order parameters does not apply in the vicinity of abrupt boundaries. This invalidates quasiclassical equations close to the boundaries and makes it necessary to complement them with appropriate boundary conditions. The conditions have been obtained for Andreev amplitudes in Ref. 34 and rederived later by various methods (see, e.g., Ref. 35). The boundary conditions for Andreev amplitudes at a plane interface can be written in the following form:

$$\begin{pmatrix} \Psi_-^l \\ \Psi_+^r \end{pmatrix} = \begin{pmatrix} \check{S}_{11} & \check{S}_{12} \\ \check{S}_{21} & \check{S}_{22} \end{pmatrix} \begin{pmatrix} \Psi_+^l \\ \Psi_-^r \end{pmatrix}. \tag{21}$$

Here, Ψ denotes a collection of Andreev amplitudes. For example, in the $(\boldsymbol{k}_F, \boldsymbol{k}_F + \boldsymbol{Q})$ representation it contains eight amplitudes $\Psi_j^T = (\tilde{u}_{j\sigma}(\boldsymbol{k}_F), \tilde{u}_{j\sigma}(\boldsymbol{k}_F + \boldsymbol{Q}), \tilde{v}_{j\bar{\sigma}}(\boldsymbol{k}_F), \tilde{v}_{j\bar{\sigma}}(\boldsymbol{k}_F + \boldsymbol{Q}), \tilde{u}_{j\bar{\sigma}}(\boldsymbol{k}_F), \tilde{u}_{j\bar{\sigma}}(\boldsymbol{k}_F + \boldsymbol{Q}), \tilde{v}_{j\sigma}(\boldsymbol{k}_F), \tilde{v}_{j\sigma}(\boldsymbol{k}_F + \boldsymbol{Q}))$. The superscripts $l(r)$ indicate that the amplitudes are taken on the left (right) side of the boundary. The subscripts $\pm$ in the amplitudes denote the sign of the Fermi velocity components $v_{F,x}(\boldsymbol{k}_F)$ or $v_{F,x}(\boldsymbol{k}_F + \boldsymbol{Q})$ for electrons. Thus, the solutions entering the left- and right-hand sides of Eq. (21) are connected at the interface by the normal-state scattering $\mathcal{S}$ matrix: $\mathcal{S} = \|\check{\mathcal{S}}_{ij}\|$ $[i(j) = 1, 2]$. This matrix $\check{\mathcal{S}}_{ii}$ contains the reflection amplitudes of normal-state quasiparticles from the interface in ith half space, whereas $\check{\mathcal{S}}_{ij}$ with $i \neq j$ incorporates the transmission amplitudes of normal-state quasiparticles from side j. In the $(\boldsymbol{k}_F, \boldsymbol{k}_F + \boldsymbol{Q})$ representation, each component $\check{\mathcal{S}}_{ij}$ $[i(j) = 1, 2]$ in the matrix $\mathcal{S}$ is an 8×8 matrix in the eight-dimensional product space of particle-hole, spin and $(\boldsymbol{k}_F, \boldsymbol{k}_F + \boldsymbol{Q})$ variables. We introduce the Pauli matrices ρ_α, τ_α, and σ_α, which operate in $\{\boldsymbol{k}_F, \boldsymbol{k}_F + \boldsymbol{Q}\}$ space, particle-hole space, and spin space, respectively.

The normal-state $\mathcal{S}$ matrix is diagonal in particle-hole space

$$\check{S} = \begin{pmatrix} \check{S}_{11} & \check{S}_{12} \\ \check{S}_{21} & \check{S}_{22} \end{pmatrix} = \hat{S}\frac{1 + \tau_z}{2} + \tilde{S}\frac{1 - \tau_z}{2}. \tag{22}$$

If the AF order parameter does not change its direction, one can take a quantization axis along $\boldsymbol{m}$. In this case up and down spin states are eigenstates of the BdG and Andreev equations, which are formulated separately for each electron spin orientation as given in Eqs. (4), (6)–(9), (13), and (14). Then the associated $\mathcal{S}$ matrix turns out to be diagonal also in spin space, and the boundary conditions reduce to the following equalities:

$$\begin{aligned} \tilde{u}_{\sigma,-}^{\alpha,l} &= \sum_\beta (S_{11,\sigma}^{\alpha\beta}\tilde{u}_{\sigma,+}^{\beta,l} + S_{12,\sigma}^{\alpha\beta}\tilde{u}_{\sigma,-}^{\beta,r}), \\ \tilde{u}_{\sigma,+}^{\alpha,r} &= \sum_\beta (S_{21,\sigma}^{\alpha\beta}\tilde{u}_{\sigma,+}^{\beta,l} + S_{22,\sigma}^{\alpha\beta}\tilde{u}_{\sigma,-}^{\beta,r}), \\ \tilde{v}_{\sigma,-}^{\alpha,l} &= \sum_\beta (\tilde{S}_{11,\sigma}^{\alpha\beta}\tilde{v}_{\sigma,+}^{\beta,l} + \tilde{S}_{12,\sigma}^{\alpha\beta}\tilde{v}_{\sigma,-}^{\beta,r}), \end{aligned} \tag{23}$$

$$\tilde{v}^{\alpha,r}_{\sigma,+} = \sum_{\beta} (\tilde{S}^{\alpha\beta}_{21,\sigma}\tilde{v}^{\beta,l}_{\sigma,+} + \tilde{S}^{\alpha\beta}_{22,\sigma}\tilde{v}^{\beta,r}_{\sigma,-}). \quad (24)$$

Here, the superscripts α, β take the two values $k_{F,y}$, $k_{F,y}+Q_y$.

As an example, we apply in the following the quasiclassical approach to analytical calculations of the subgap spectrum of quasiparticle interface states near a (110) SC/AF interface in the absence of potential barriers. A detailed self-consistent study of quasiparticle states at interfaces with antiferromagnets will be presented below in Secs. IV and V. Let an *s*-wave superconductor and an antiferromagnet, separated with the (110) interface, occupy separately the right half spaces ($j>0$) and the left ($j\leqslant 0$) half spaces of the square lattice. Assuming $|E|<|\Delta|\ll|m|$, $|v_{F,x}|/a$, we use the Andreev equations only in the superconducting region and apply the boundary conditions at the superconductor-antiferromagnet interface. Wave functions for quasiparticles with energies below the superconducting gap decay exponentially with increasing distance from the interface. Solving the Andreev equations, one can easily find the standard two component solutions $\tilde{\psi}^{r}_{\sigma,\pm}(\boldsymbol{k}_F)=(\tilde{u}^{r}_{\sigma,\pm}(\boldsymbol{k}_F),\tilde{v}^{r}_{\bar{\sigma},\pm}(\boldsymbol{k}_F))$ taken in the right half space of the boundary

$$\tilde{\psi}^{r}_{\sigma,\pm}(\boldsymbol{k}_F) = C_{\pm}\begin{pmatrix} E \pm i\sqrt{\Delta_s^2 - E^2} \\ -\Delta_s \end{pmatrix}. \quad (25)$$

Reflection amplitudes for electrons r^e_σ and holes r^h_σ, which enter the quasiclassical boundary conditions, are taken for the normal-metal state of the superconducting region at the Fermi surface. An AF/*N* boundary is impenetrable for normal-metal quasiparticles with energies below the antiferromagnetic gap, even in the absence of any interface potentials (i.e., for a transparent interface). Hence, the corresponding transmission amplitudes vanish and the complex reflection amplitudes for electrons and holes have the unit modulus $|r^e(\boldsymbol{k}_F)|=|r^h(\boldsymbol{k}_F)|=1$. Further, if $\tilde{\psi}^{r}_{\sigma}(\boldsymbol{k}_F)$ represents an outgoing solution in the case of a (110) interface, then $\tilde{\psi}^{r}_{\sigma}(\boldsymbol{k}_F+\boldsymbol{Q})$ is the incoming solution and vice versa. Here, $\boldsymbol{Q}=(\pm\sqrt{2}\pi,0)$ only has a nonzero *x* component. For this reason, it is convenient to formulate the boundary conditions for the (110) interface indicating explicitly only the k_y component

$$\tilde{\psi}^{r}_{\sigma,+}(k_y) = \left(r^e_\sigma(k_y)\frac{1+\hat{\tau}_z}{2} + r^h_\sigma(k_y)\frac{1-\hat{\tau}_z}{2}\right)\tilde{\psi}^{r}_{\sigma,-}(k_y). \quad (26)$$

A relation between $r^e_\sigma(\boldsymbol{k}_F)$ and $r^h_\sigma(\boldsymbol{k}_F)$ follows from the fact that the quantity $-[u_{-\sigma}(\boldsymbol{k}_F)]^*$ represents the wave function $v_{\bar{\sigma}}(\boldsymbol{k}_F)$ for a hole with energy $-E$ from one spin subband if $u_\sigma(\boldsymbol{k}_F)$ is the wave function for an electron with energy E from the other spin subband. Under the condition $\Delta\ll t$, one can consider the reflection amplitudes at subgap energies $\pm E$ as taken at the Fermi surface. Accounting additionally for the fact that incoming and outgoing waves for holes are interchanged as compared with the case of electrons, we find for normal-metal electrons and holes at the (110) AF/*N* interface: $r^h_\sigma=(r^{e^*}_{\bar{\sigma}})^{-1}$. This condition simplifies because of the equalities $|r^e(\boldsymbol{k}_F)|=|r^h(\boldsymbol{k}_F)|=1$: $r^h_\sigma=r^e_{-\sigma}$. Eventually, applying the boundary conditions (26) to the solution (25), we get

$$C_+(E+i\sqrt{\Delta_s^2-E^2}) = r^e_\sigma(\boldsymbol{k}_F)C_-(E-i\sqrt{\Delta_s^2-E^2}),$$

$$C_+ = r^e_{-\sigma}(\boldsymbol{k}_F)C_-. \quad (27)$$

This equation determines the energies of the bound states at a (110) AF/sSC interface. In order to present the energy in a convenient form, we divide the reflection amplitude into two parts $r^e_\sigma(\boldsymbol{k}_F)=r_{sp}+r_{Q,\sigma}$, which are symmetric and antisymmetric with respect to spin inversion, respectively. The first part r_{sp} is actually spin independent and can be considered as the contribution to the reflection amplitude from the specular reflection channel. The contribution to the reflection amplitude from the spin-dependent *Q* reflection differs in symmetry from the specular reflection part. This is the part antisymmetric in σ, $r_{Q,\sigma}$, which is an imaginary quantity. The phase of $r_{Q,\sigma}$ differs by π for spin up and down quasiparticles.[25] It follows from the definition given and the condition $|r^e_\sigma(\boldsymbol{k}_F)|=1$ that reflection coefficients $R_{sp}=|r_{sp}|^2$ and $R_Q=|r_{Q,\sigma}|^2$ satisfy the relation $R_{sp}+R_Q=1$. With these quantities, we obtain from Eq. (27) the following bound state energies at the (110) AF/sSC interface:

$$E = \pm\Delta_s\sqrt{R_{sp}(\boldsymbol{k}_F)}. \quad (28)$$

If a *d*-wave superconductor occupies the right half space instead of the *s*-wave one, the expression for $\tilde{\psi}^{r}_{\sigma,\pm}(\boldsymbol{k}_F)$ in Eq. (25) is modified with the substitution $\Delta_s\rightarrow\pm\Delta_d(\boldsymbol{k}_F)$. As a result, we obtain the spectrum of the bound states at the (110) AF/dSC interface

$$E = \pm\Delta_d(\boldsymbol{k}_F)\sqrt{R_Q(\boldsymbol{k}_F)}. \quad (29)$$

The specific expressions for the normal-state reflection amplitudes can be found for the (110) AF/*N* interface along the standard way by solving the Schrödinger equations for electrons in the left and the right half spaces and constructing incoming and outgoing solutions in the normal-metal region, as well as the exponentially decaying solution in the antiferromagnetic region for electrons with energies below the antiferromagnetic gap. The reflection amplitude is fixed after substituting the bulk solutions to the equations taken at lines where the nearest neighbor hopping mixes the normal-metal and the antiferromagnetic regions,

$$r_{Q,\sigma}(\boldsymbol{k}_f) = -i\sigma\left[1+\left(\frac{ma}{\sqrt{2}v_{F,x}(k_y)}\right)^2\right]^{-1/2},$$

$$r_{sp}(\boldsymbol{k}_F) = \left[1+\left(\frac{\sqrt{2}v_{F,x}(k_y)}{ma}\right)^2\right]^{-1/2}, \quad (30)$$

where $v_{F,x}(k_y)=2\sqrt{2}ta\cos(k_y/\sqrt{2})$.

Substituting Eq. (30) into Eqs. (28) and (29), we come to the results obtained in Ref. 25. We note now that the (110) interface represents a special situation, when the normal state Fermi velocity for the half-filled lattice has only a $v_{F,x}$ component, which is perpendicular to the surface. Hence, outgoing and incoming normal-metal quasiparticles move only along or opposite to the surface normal. The quasiparticle trajectory of this kind is intrinsic to the specular reflection

channel. However, Q reflection takes place in this particular case along the same quasiparticle trajectory. For this reason, specular and Q reflections make coherent contributions to the total reflection amplitude $r_\sigma^e(\boldsymbol{k}_F)=r_{sp}+r_{Q,\sigma}$. For different interface orientations, for example, for the (100) interface, specular and Q reflection takes place along different trajectories and do not interfere with each other.

In the absence of interface potentials specular reflection of quasiparticles arises entirely due to a mismatch of Fermi velocities in the AF and the sSC. Since normal-metal states are presumably identical in the left and right half spaces under the conditions $\Delta \ll m,t$ the mismatch in the model is controlled by the parameter m/t. As is seen from Eq. (30), $r_{sp}\to 1$ when the antiferromagnetic gap is large, $|m| \gg 4t\cos k_y$. At the same time Q reflection becomes dominant in the opposite limit $|m| \ll 4t\cos k_y$, taking place at energies below the antiferromagnetic gap $|E|<|m|$. The quasiparticle bound state energy (28) at the AF/sSC interface is almost zero in the limit $|E| \ll \Delta_s$, whereas the bound state (29) at the AF/dSC interface lies very close to the edge of the superconducting gap.

IV. QUASIPARTICLE STATES AT SC/AF INTERFACES

In this section we study quasiparticle spectra and the corresponding local density of states in the vicinity of AF/SC interfaces based on our self-consistent approach outlined above. We consider (100) and (110) interfaces between AF and either s-wave or d-wave superconductors. The coupling constants are site dependent with

$$U_i = U \quad \text{for } i \leqslant 0, \tag{31}$$

$$V_i = V \quad \text{for } i > 0, \tag{32}$$

and zero elsewhere. In the following we will typically be studying finite systems of length $N=100-200$ along the x axis. The k_y sum is performed explicitly by using 400 points in the Brillouin zone. The interface is always positioned at the bond in the middle of the system and the potential h_i is only nonzero on the two sites immediately adjacent to the interface. We apply open boundary conditions equivalent to an impenetrable wall at each end of the system.

A. The s-wave superconductor-antiferromagnet (100) interface

We begin with the AF/sSC (100) situation since Q reflection is expected to lead to low-energy bound states for this particular interface orientation.[25] As is well known, nonmagnetic interfaces do not break s-wave Cooper pairs in their vicinity. In contrast, ferromagnetic as well as antiferromagnetic interfaces are pair breaking, in general, even for s-wave superconductors since they break time-reversal symmetry. This is analogous to the difference between effects of nonmagnetic and magnetic impurities in s-wave superconductors. In Fig. 5 we show the self-consistent suppression of the magnetization M_i and the pairing amplitude F_{ii} near the (100) interface for various values of superconducting and antiferromagnetic coupling constants. As seen, the healing length on each side of the interface decreases with increasing

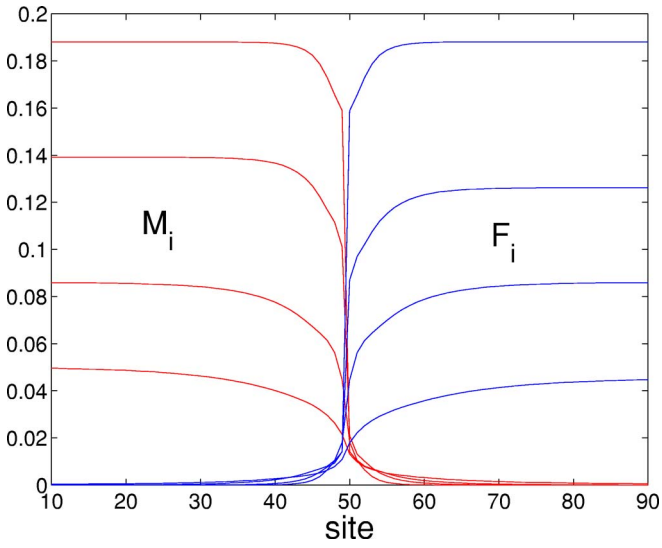

FIG. 5. (Color online) Self-consistent spatial dependence of the absolute values of the magnetization M_i and the pairing amplitude F_{ii} near a (100) interface. Parameters: $\mu=0$ and, from top to bottom, ($U=2.0t$, $V=2.0t$), ($U=1.6t$, $V=1.5t$), ($U=1.2t$, $V=1.2t$), and ($U=0.93t$, $V=0.9t$).

amplitude of the order parameter in agreement with the behavior of the respective magnetic and superconducting coherence lengths $\sim\hbar v_{F,x}/|m|, \hbar v_{F,x}/\Delta_s$. We find a correlation between the strength of the suppression of order parameters and the energy of the Andreev bound state arising near the AF/sSC interfaces. The lower the (positive) energy of the subgap state, the stronger the suppression of both order parameters at the interface, at least in simple cases which have been studied.

In Fig. 6 we plot the quasiparticle spectrum as obtained from the eigenvalues of the BdG equations (6) and (7). Naturally, bound states present at the interface show up inside the

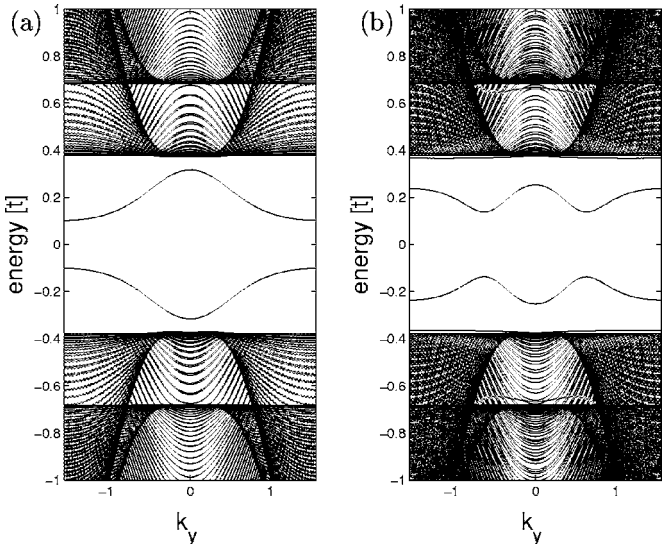

FIG. 6. Eigenvalues for the (100) AF/sSC interface as a function of k_y for $\mu=0.0$, $U=2.7t$, $V_s=2.0t$, and $h=0.0$ (a) and $h=2.0t$ (b). Here, one sees explicitly the presence and dispersion of the bound state band inside the gap.

main gap of the spectrum as a distinct band, which disperses with the momentum component k_y along the interface. The two gap edges seen in Fig. 6 are associated with the superconducting (lesser) and the antiferromagnetic (larger) gaps.

We have calculated the bound state spectrum also analytically, assuming $\Delta_s \ll m,t$. Solving the Andreev equations for the superconducting region and applying appropriate boundary conditions, we obtain the two dispersive energies of quasiparticle Andreev bound states for the (100) AF/sSC interface. The spectrum is symmetric with respect to the zero level and can be described with a reflection coefficient $R_{sp}(k_y)$ for quasiparticles in the specular reflection channel: $E(k_y)=\pm\Delta_s\sqrt{R_{sp}(k_y)}$. This expression actually coincides with Eq. (28) derived in Sec. III for the (110) interface although the explicit expression for the reflection coefficient differs for the two orientations. A calculation of the reflection coefficient $R_{sp}(k_y)$ for the (100) AF/sSC interface in the absence of potential barriers leads to the following explicit expression for energies of the Andreev bound states:

$$E(k_y) = \pm\Delta_s\left(\frac{A(k_y)+\sqrt{A^2(k_y)+4\left(\frac{m}{2t}\right)^2}}{A(k_y)+2\sin^2 k_y+\sqrt{A^2(k_y)+4\left(\frac{m}{2t}\right)^2}}\right)^{1/2}, \tag{33}$$

where

$$A(k_y)=\left(\frac{m}{2t}\right)^2-\sin^2 k_y. \tag{34}$$

The dispersion shown in Fig. 6(a) can be verified to agree well with the expression in Eq. (33) within the accuracy $\pm(\Delta/t)^2$. Equation (33) is very similar to Eq. 7 of Ref. 36 and can be obtained from there simply by substituting the magnetic m and s-wave Δ_s order parameters for the charge density wave W_s and d-wave Δ_d order parameters, respectively. As follows from Eq. (33), the quasiparticle subgap state becomes a dispersionless zero-energy state if one additionally assumes $m \ll t$ and disregards terms less or of the order of $(m/t)^2$. This limiting case corresponds to the zero-energy solution found from the quasiclassical Andreev equations applied to both superconducting and antiferromagnetic regions under the conditions $m,\Delta_s \ll t$.[25]

The differential tunneling conductance measured, for instance, by scanning tunneling microscopy (STM) experiments is proportional to the local density of states.[37] Therefore, it is important to calculate the LDOS, given by

$$N_i^\alpha(\omega) = -\frac{\mathrm{Im}}{\pi}\sum_{nk_y\sigma}\left[\frac{|u^\alpha_{n,i,\sigma}(k_y)|^2}{\omega-E_{nk_y\sigma}-i\Gamma}+\frac{|v^\alpha_{n,i,\sigma}(k_y)|^2}{\omega+E_{nk_y\sigma}-i\Gamma}\right], \tag{35}$$

where $\alpha=A,B$ indicates the magnetic sublattice and Γ is an artificial broadening which in the following is set to $\Gamma=0.02t$. For the (100) interface, we find $N_i^A(\omega)=N_i^B(\omega)$. In plots of the resulting LDOS we expect any bound states to result in additional peaks inside the gap of the bulk AF and SC. These peaks should be localized near the interface. This is indeed the case for the (100) AF/sSC interface, as can be seen from Fig. 7. Here, the two center LDOS scans in both 7(a) and 7(b) are at the interface while the top (bottom) five scans are moving into the SC (AF).

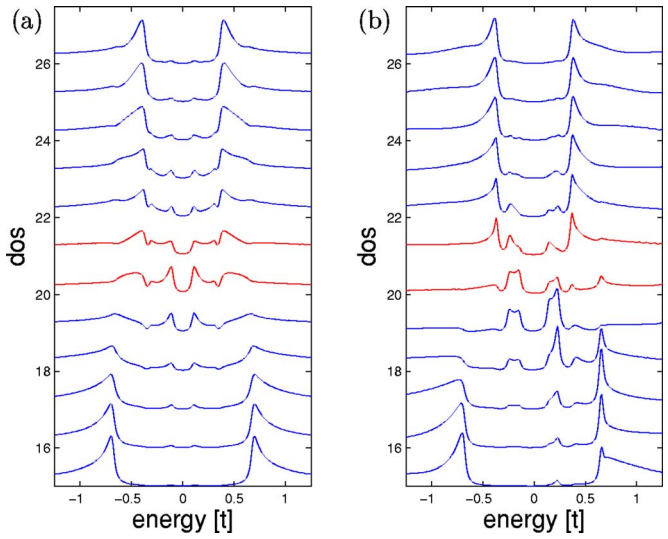

FIG. 7. (Color online) LDOS corresponding to the same parameters as in Fig. 6. The interface bound states result in subgap peaks in the LDOS near the interface region. The two center LDOS scans in both (a) and (b) are at the interface while the top (bottom) five scans are into the SC (AF). The lines are off-set for clarity.

Additional potentials $h \neq 0$ present near the interface can strongly enhance specular reflection at the expense of the Q reflection. There are several consequences of the interface potential for Andreev bound states present in the system. First, potentials tend to suppress the bound states resulting from Q reflection and move their positions towards the gap edge. As expected, in the limit $h \gg t$ we always find that the Q reflection bound states have been pushed into the continuum. Second, in the regime where h is of the order of t, we find that the main effect of the specular reflection channel is to cause a stronger dispersion of the bound state energy. One can identify additional extrema in the wave vector dependence of the bound state energy $E(k_y)$. A typical example is seen in Fig. 6(b) where $h=2.0t$. The new stationary points in the dispersion lead to additional LDOS peaks near the interface as seen in Fig. 7(b). In the LDOS we also see that the particle-hole symmetry is broken when $h \neq 0$, whereas the quasiparticle spectrum is still symmetric with respect to the Fermi level. A similar asymmetry between positive and negative bias in the LDOS will be present when starting from a particle-hole asymmetric band, i.e., when $\mu \neq 0$. For the sake of clarity, the results presented below are for the particle-hole symmetric nested band where $\mu=0$ and any asymmetry will only result from a nonzero interface potential h.

It is interesting to investigate the importance of the suppression of the order parameters near the interface resulting from the self-consistency. Figure 8 shows the bands and the corresponding LDOS for a non-self-consistent calculation with step-function fields: $m_i^A=-m_i^B=m_0\Theta(-i)$, $\Delta_s=\Delta_0\Theta(i)$ with $m_0=0.7t$, and $\Delta_0=0.4t$. Clearly, the results are very

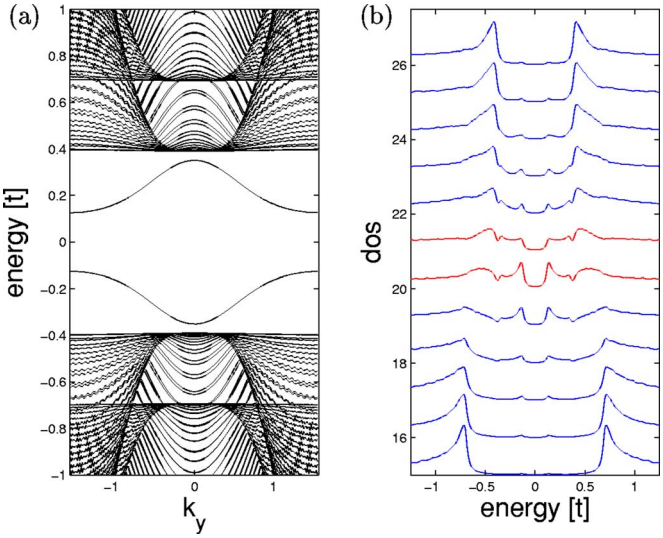

FIG. 8. (Color online) Non-self-consistent spectrum and LDOS corresponding (roughly) to the same parameters as in Fig. 6(a) but with step-function spatial dependence of M_i and F_{ii}. These results are basically identical to those shown in Fig. 6(a), verifying that it is the Q reflection, not the order parameter suppression, that generates the subgap states.

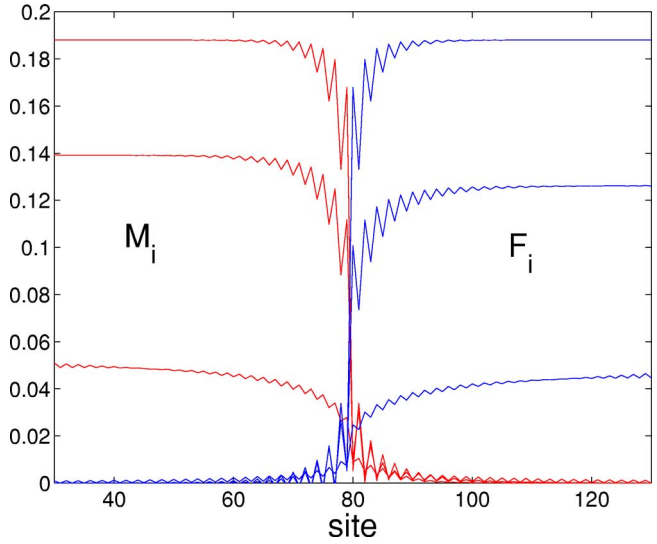

FIG. 10. (Color online) Spatial dependence of the self-consistent results for the absolute value of the magnetization M_i and pairing amplitude F_{ii} for the AF/sSC (110) interface orientation. Parameters: $\mu=0$ and (top) $U=2.0t$, $V=2.0t$, (middle) $U=1.6t$, $V=1.5t$, and (bottom) $U=0.93t$, $V=0.9t$.

similar to those shown for $h=0$ in Figs. 6(a) and 7(a), respectively. This result applies also to the other interfaces studied below: in general the self-consistency has only minor effects on the bound states resulting from Q reflection. It can, on the other hand, depending on specific parameters, induce new bound states close to the gap edge.

As a final point in this section, we verify the bound nature of the subgap states by showing explicitly the spatial dependence of the eigenstates corresponding to the subgap band in, e.g., Fig. 6(a). This is done in Fig. 9, where we plot $|u_i^A(k_y)|^2=|u_i^B(k_y)|^2$ as a function of the x component of the unit cell near the interface for $k_y=0.0$ and $k_y=0.25\pi$. Clearly, the wave functions are seen to be bound to the interface region.

B. The *s*-wave superconductor-antiferromagnet (110) interface

Unlike the (100) interface studied in the preceding section, in the (110) case all sites at the interface belong to the same sublattice, so that the interface layer (chain) itself is ferromagnetically ordered. Up and down magnetizations alternate only along the interface normal, i.e., the x direction as seen from Fig. 2. For this reason some characteristic properties of AF/sSC (110) interfaces could naively be expected to be reminiscent of the properties of superconductor-ferromagnetic boundaries. For example, Cooper pair wave functions are known to decay into the ferromagnet adjacent to the superconductor, manifesting at the same time spatial oscillations.[6,38] The oscillations are known to be induced by the difference between the momenta of spin up and down quasiparticles with the same energy.[39] These oscillations in the SC/F proximity effect are related to those in the Fulde-Ferrell-Larkin-Ovchinnikov (FFLO) superconducting phase.[40]

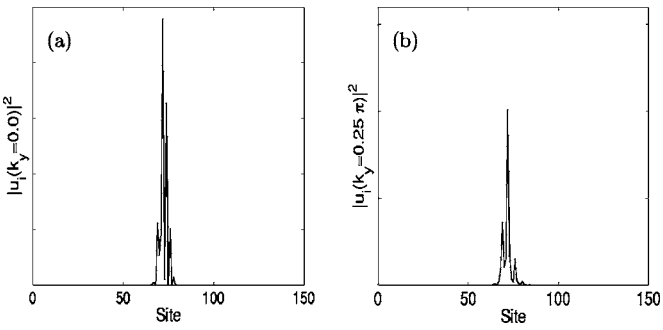

FIG. 9. Amplitude of $|u_i^A(k_y)|^2$ as a function of the x component of the unit cell i corresponding to the bound state in Fig. 6(a) when $k_y=0.0$ (a) and $k_y=0.25\pi$ (b), respectively.

In Fig. 10 we show the obtained self-consistent spatial profiles of the magnetization M_i and the pairing amplitude F_{ii} near the (110) AF/sSC interface region for various coupling strengths. Both the magnetization and the pairing amplitude display an oscillatory decaying behavior near the interface. The oscillations have an even-odd character, i.e., they are not present within each separate magnetic sublattice. Thus, the oscillations in Fig. 10 are not equivalent to FFLO oscillations, but simply induced by the AF staggered ordering. The characteristic scales for suppression of the order parameters are seen to be the corresponding coherence lengths of the antiferromagnet and the superconductor. We find that an additional potential at the interface decreases both the decay length and the amplitude of the oscillations on both sides of the interface.

The dispersion of the subgap energies at (110) AF/sSC interfaces are described analytically by Eqs. (28) and (30) within the non-self-consistent quasiclassical approach. In Fig. 11(a) we plot the numerically determined self-consistent (spin up) eigenbands for the (110) AF/sSC interface. The

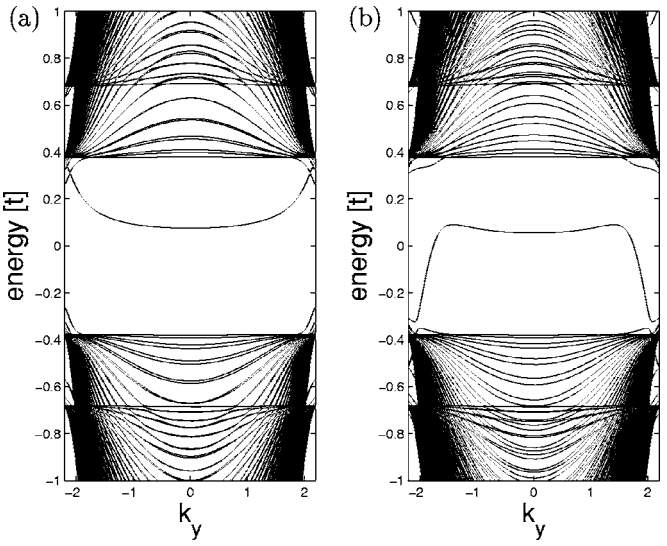

FIG. 11. Spin up eigenvalues resulting from the Bogoliubov–de Gennes equations in the case of a (110) AF/sSC interface. The parameters are $U=2.7t$, $V=2.0t$, and $h=0.0$ for (a) and $h=1.0t$ for (b). The bands shown here correspond to $(u_\uparrow, v_\downarrow)$. The bands associated with $(u_\downarrow, v_\uparrow)$ are identical to the bands shown here upon mirror reflection around $E=0$.

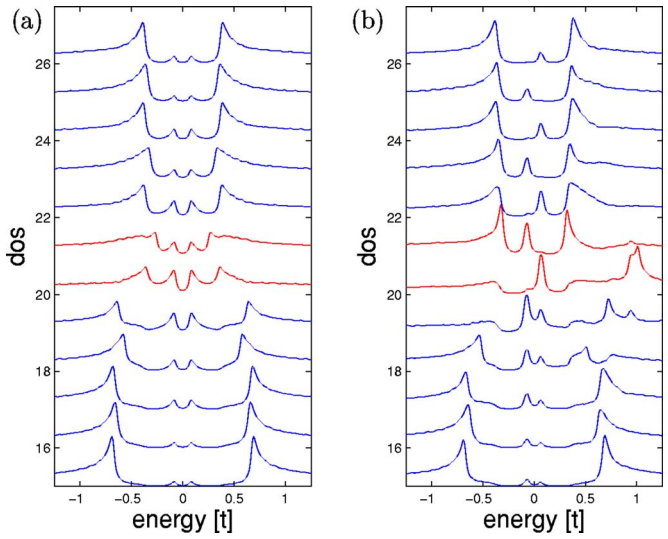

FIG. 12. (Color online) LDOS near the (110) AF/sSC interface corresponding to the parameters used in Fig. 11. The two center LDOS scans in both (a) and (b) are at the interface while the top (bottom) five scans are the LDOS upon moving into the SC (AF). The lines are offset for clarity.

dispersion of the main bound state can be checked to yield excellent agreement with the result in Eq. (28). Positive and negative energies correspond there to spin up and down quasiparticles, respectively. Thus, at low temperatures only spin down quasiparticle Andreev states will be occupied. Strongly spin-discriminated Andreev states together with the alternating magnetization of chains, which are parallel to the (110) interface, are at the origin of the even-odd oscillations of the order parameters shown in Fig. 10. It is worth noting that spin polarized Andreev states are compatible with singlet spin structure of Cooper pairs.[9] Whereas the electron and the Andreev reflected hole belong to different spin subbands and have opposite Zeeman energies, they possess identical spin polarization. Since they have also almost opposite velocities, they do not carry together any spin current except for special cases.[41]

At the edge of the Brillouin zone we find new high-energy subgap states. By comparing to non-self-consistent calculations with steplike spatial order parameter dependence, we have found that these states are related to the self-consistent order parameter suppression near the interface. When including a potential at the interface, the structure of the dispersion of the subgap states becomes more complicated. In Fig. 11(b) we show an example where $h=t$. When the potential becomes too large, $h \gg m, \Delta$, the specular reflection channel completely dominates the Q reflection and all bound states are pushed out of the gap into the continuum.

The spin-summed LDOS corresponding to the results shown in Figs. 11(a) and 11(b) is shown in Fig. 12. Since in the (110) case sites A and B from the same cell are at different distances from the interface, $N_i^A(\omega)$ and $N_i^B(\omega)$ differ from each other. Each of Figs. 11(a) and 11(b) display $N_i^A(\omega)$ and $N_i^B(\omega)$ jointly, i.e., show the LDOS for all sites along the x axis. As expected, the bound states again show up as peaks in the LDOS close to the interface. The states at the Brillouin zone edge can give rise to higher energy peaks. The main influence of the potential scattering is to break the particle-hole symmetry present in the LDOS in Fig. 12(a). In particular, as seen from Fig. 12(b), the presence of a potential h can lead to distinct even(odd) amplitude modulations of the bound state LDOS peaks into the superconductor.

C. The *d*-wave superconductor-antiferromagnet (100) interface

The electronic structure of interfaces formed by d-wave superconductors and antiferromagnets is an important problem relevant to, e.g., the high temperature superconductors where AF and dSC order dominate the phase diagram. A qualitative difference between the properties of AF/sSC and AF/dSC interfaces arises from the fact that the quasiclassical d-wave order parameter $\Delta_d^j(\boldsymbol{k}_f)$ changes sign in a Q reflection event for any interface orientation, $\Delta_d(\boldsymbol{k}_F+\boldsymbol{Q})=-\Delta_d(\boldsymbol{k}_F)$. This change of sign can strongly weaken the effect of phase difference of reflection coefficients for spin up and down quasiparticles, which is close to π in the limit $\Delta, m \ll t$. For this reason, low-energy interface bound states $E_B(\boldsymbol{k}_F) \ll \min\{m, \Delta_{\text{bulk}}(\boldsymbol{k}_F)\}$ existing at AF/sSC interfaces under the conditions $\Delta_s, m \ll t$, do not exist at AF/dSC interfaces with arbitrary orientation.[25] In this section we demonstrate results of self-consistent numerical calculations for the spatial profiles of superconducting and antiferromagnetic order parameters, the quasiparticle spectrum, and the associated LDOS in the vicinity of (100) AF/dSC interfaces.

Figure 13 shows a typical result for the suppression of M_i and F_i near the interface. Here, we plot the d-wave pairing amplitude defined on-site in the usual way from the four surrounding links $F_i=(F_{i,i+a}+F_{i,i-a}-F_{i,i+b}-F_{i-b})$. Comparing Fig. 13 and Fig. 5, one can notice weaker pair breaking effects on the scale of the respective coherence length for the

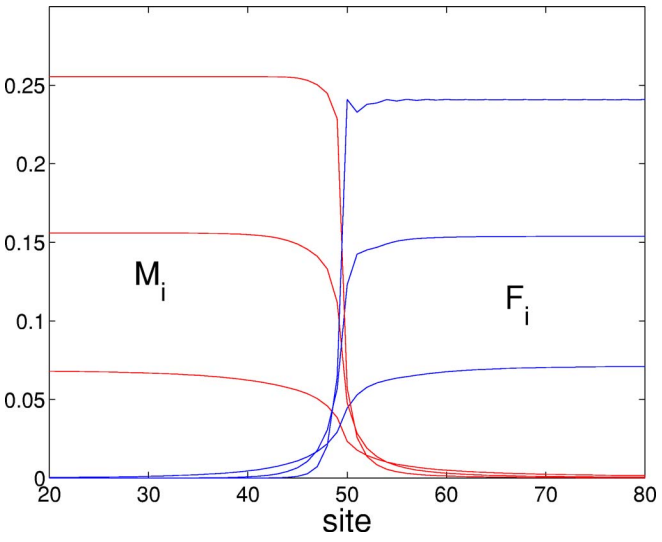

FIG. 13. (Color online) Spatial dependence of the self-consistent results for the absolute value of the magnetization M_i and pairing amplitude F_i for the AF/dSC (100) orientation. Parameters: $\mu=0$, and (top to bottom) $U=2.7t$, $V=2.0t$; $U=1.7t$, $V=1.0t$; and $U=1.1t$, $V=0.5t$.

AF/dSC (100) interface compared to the AF/sSC interface. This is associated with lower bound state energies at AF/sSC interfaces. We find similar results for the (110) AF/dSC interface studied in the next section. Contrary to the (110) AF/sSC case, the order parameters exhibit a rather smooth suppression near a (100) or (110) AF/dSC interface, i.e., the order parameter oscillations are absent. This correlates with the absence of a spin discrimination in the quasiparticle subgap spectrum generated by the (110) AF/dSC boundary.

The eigenbands for two different parameter sets are shown in Fig. 14. The left figure shows the result without any potential at the interface. Here, a subgap band exists close to the edge of the continuum. We find that the larger the ratio m/Δ, the closer the subgap band is to the gap edge.

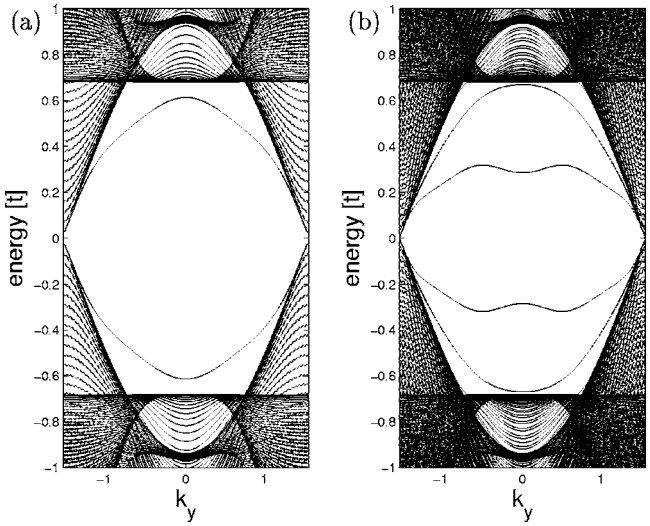

FIG. 14. Eigenbands for the AF/dSC (100) interface as a function of k_y. Parameters: $U=2.7t$, $V=2.0t$, $\mu=0$, and $h=0.0$ (a) and $h=1.0t$ (b).

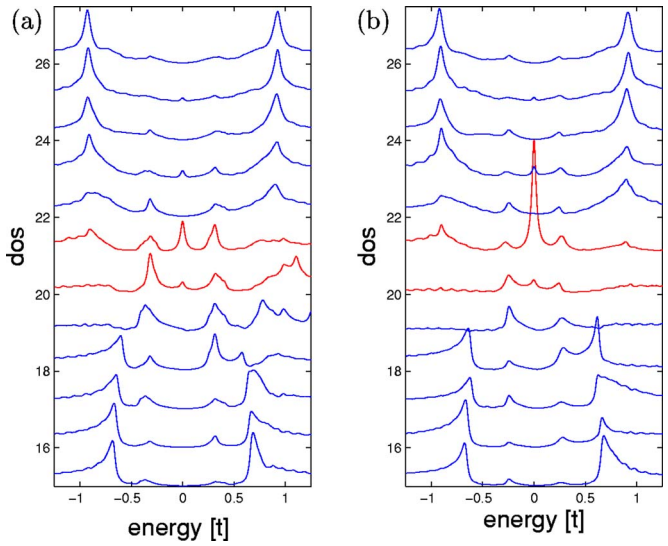

FIG. 15. (Color online) LDOS corresponding to the plots shown in Fig. 14. The two center LDOS scans in both (a) and (b) are at the interface while the top (bottom) five scans shows the LDOS when moving into the SC (AF).

This agrees with Ref. 25, where it was demonstrated that there are no interface bound states on AF/dSC (100) interfaces in the limit $m \gg \Delta$. Only upon decreasing the ratio m/Δ does a bound state gets peeled off the continuum, as seen in Fig. 14(a). The band is degenerate and will be split by a nonzero potential $h \neq 0$ as seen in Fig. 14(b). This is accompanied by the appearance of additional extrema in the dispersion of a lower band. Although with increasing h a lower band first becomes closer to the Fermi level than for $h=0$, its position depends nonmonotonically on h and never approaches zero energy. When $h \gg t$, both bound state bands are pushed into the continuum. The results of non-self-consistent calculations are very similar to the results shown in Fig. 14, it is the Q reflection channel that induces the bound states at the AF/dSC interface, not the order parameter suppression.

The LDOS corresponding the same parameters used in Fig. 14 is shown in Fig. 15. Again the new LDOS peaks arising from the bound states are sensitive to the presence of the interface potential h. When $h=0$ the bands in Fig. 14(a) close to the continuum edge gives rise to LDOS peaks near the coherence peaks. Experimentally, it may be a challenge to distinguish these bound state peaks from the coherence peaks of the bulk dSC. However, for the case when $h=1.0t$, we see that the lower band from Fig. 14(b) results in sharp LDOS peaks near the interface in the intermediate region of subgap energies.

D. The *d*-wave superconductor-antiferromagnet (110) interface

As is well known, a zero-energy Andreev bound state exists at the (110) insulator I/dSC interface generated by the sign reversal of the gap function as seen by a quasiparticle specularly scattered off the surface.[29–31] This state has been observed in the differential tunneling conductance as a conductance peak at zero bias.[42–56] In this section we study the AF/dSC interface with (110) orientation.

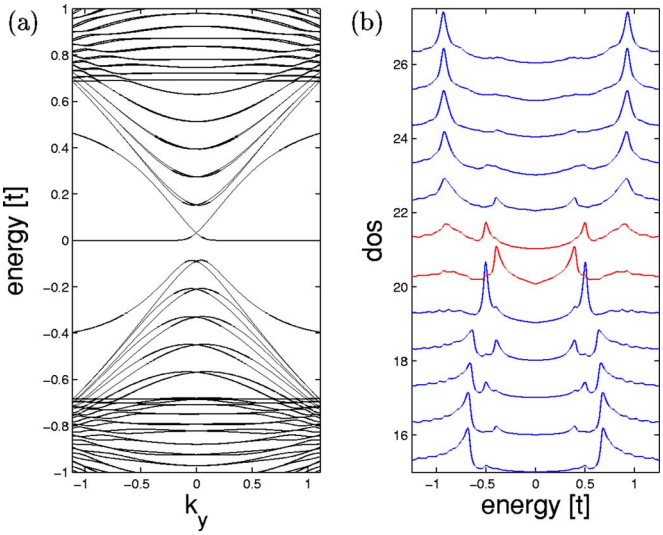

FIG. 16. (Color online) Bands and LDOS for the (110) AF/dSC interface with $U=2.7t$, $V=2.0t$, and $h=0.0$. The low-energy bands are dominated by the gap node at $k_y=0$, the Q reflection bound states and a zero energy state. The latter state is located at the dSC/I boundary at the right-most the end of our system where the open boundary conditions operate as a hard wall.

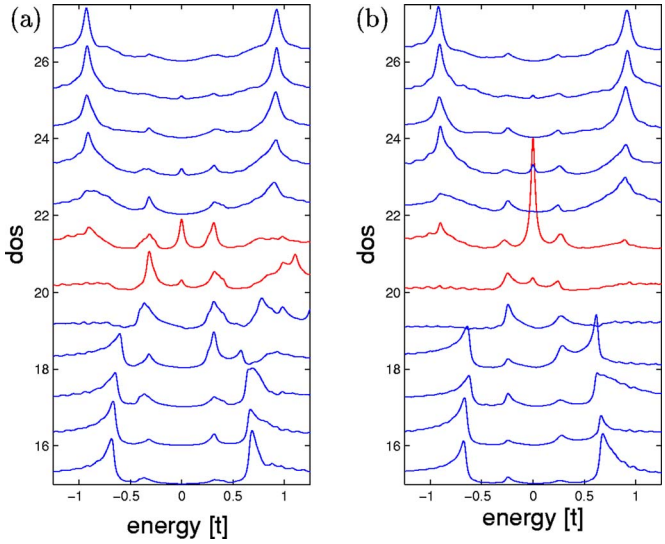

FIG. 17. (Color online) LDOS for the (110) AF/dSC interface with $\mu=0$, $U=2.7t$, $V=2.0t$, and $h=1.0t$ (a) and $h=2.0t$ (b). Again, the two center LDOS scans in both (a) and (b) are at the interface while the top (bottom) five scans show the LDOS when moving into the SC (AF). Here, one clearly sees the continuous evolution of the well-known zero energy state with increasing interface potential h.

In Fig. 16 we plot the (spin up) bands and the corresponding LDOS when $U=2.7t$, $V=2.0t$, and $h=0.0$. Since the open boundary conditions at the edges of our finite system are equivalent to a hard wall, a zero energy state (ZES) is present at the superconducting end of our system. This state, clearly seen in Fig. 16(a), is not associated with the AF/dSC interface in which we are interested. It mixes with the bound states resulting from the Q reflection at the interface, however, and causes small deviations from the expected mirror symmetry (through $E=0$) of the bound state bands. In the limit of an infinite system, this spurious effect disappears and the continuum gap node closes at $k_y=0$.

The dispersion of the subgap states in the absence of potential barriers is described analytically in Eqs. (29) and (30) assuming spatially constant order parameters $\Delta_d(\boldsymbol{k}_F) \ll m,t$. These states should move to lower energy as m increases. For our band $v_{F,x}=2\sqrt{2}ta\cos(k_y/\sqrt{2})$ and again it can be easily verified that the functional form of the self-consistent subgap band in Fig. 16(a) agrees well with Eqs. (29) and (30).

The presence of ZES at (110) I/dSC interfaces makes it interesting to plot the LDOS as a function of increased interface potential h. Figure 17 shows the evolution of the LDOS when approaching the interface in two cases where $h=t$ [Fig. 17(a)] and $h=2t$ [Fig. 17(b)]. The details of the dispersion of the subgap states are sensitive to the strength of the potential barrier at the interface, and the resulting LDOS will strongly depend on h. In the limit where $h \gg t$ the low-energy LDOS near the interface will be dominated by the ZES. However, in the regime where $h \sim t$, the ZES coexists with the Q reflection bound states as is evident from Fig. 17. This finding is relevant for the discussion of possible surface induced magnetization near I/dSC interfaces in cuprate superconductors.[24,57,58] In the case of small finite M_i near a (110) dSC surface, we would expect small sideband peaks originating from the Q reflection as seen in Fig. 17.

E. Transfer matrix method

The existence and dispersion of bound states at interfaces between SC and AF can also be conveniently formulated within a transfer matrix method designed to locate the bound states from their defining property, spatially decaying wave functions. Below, we use the same transfer matrix formalism presented in Ref. 24. In this method, one introduces a (q,ϵ)-dependent matrix $T(i+1,i)$ defined by

$$\Psi(i+1) = T(i+1,i)\Psi(i), \tag{36}$$

which transfers the spinor Ψ from site i to site $i+1$. For a model with nearest neighbor coupling Ψ takes the explicit form $\Psi(i)=(\psi(i),\psi(i-1))$, where

$$\psi(i) = (u_{k_y\sigma}(i), v_{k_y\sigma}(i), u_{k_y+\pi\sigma}(i), v_{k_y+\pi\sigma}(i)). \tag{37}$$

The associated 8×8 transfer matrix has the general form

$$T(i+1,i) = \begin{pmatrix} A & B \\ 1 & 0 \end{pmatrix}, \tag{38}$$

where A (B) denotes the 4×4 coefficient-matrix connecting $\psi(i+1)$ and $\psi(i)$ $[\psi(i-1)]$ determined from the Bogoliubov–de Gennes Equations (4).

For a typical interface there will be three distinct transfer matrices; one in the bulk magnetic region T_M, one in the bulk SC region T_{SC}, and one associated with transfer through the interface T_I. By diagonalizing T_M and T_{SC} one determines whether eigenstates decay, grow or propagate from the interface depending on whether the eigenvalues are less than,

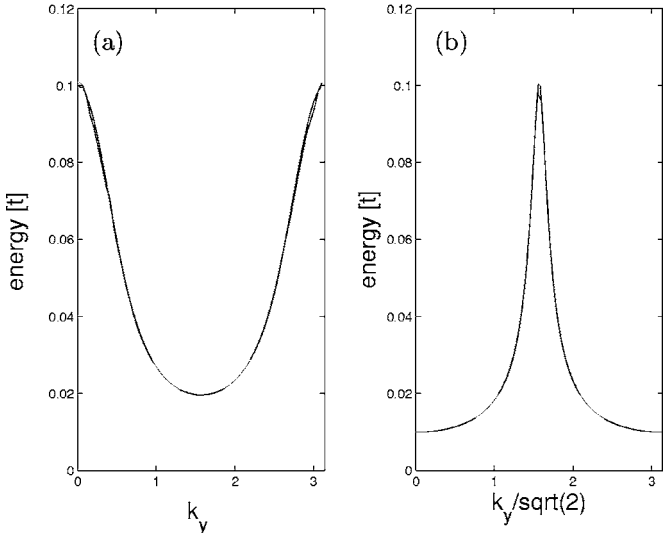

FIG. 18. Comparison of the dispersion obtained for the 100 (a) and 110 (b) AF/sSC interface form the transfer matrix method and the result of Eq. (33) (a) or Eqs. (28) and (30) (b), respectively. There appears to be only one plot in each figure here because of the excellent agreement between these two methods.

larger or equal to one, respectively. Here, decaying and growing refer to propagation along the x axis.

Let PE_M denote the matrix obtained after propagating the eigenvectors of the bulk magnetic transfer matrix through the interface. Then we can define a matrix A given by

$$PE_M = E_{SC}A, \tag{39}$$

where E_{SC} is the matrix containing the eigenvectors of the bulk superconducting region as column vectors. Let S_g^M and S_g^{SC} denote the subspace of growing eigenstates of PE_M and E_{SC}, respectively. Consider the following linear combination of the *growing* states of PE_M:

$$\sum_{i\in S_g^m} \beta_i |PE_M i\rangle = \sum_{i\in S_g^m}\sum_{j\in S_g^{SC}} \beta_i A_{ji}|E_{SC}j\rangle = \sum_{j\in S_g^{SC}} \left(\sum_{i\in S_g^M} A_{ji}\beta_i\right) \times |E_{SC}j\rangle. \tag{40}$$

From Eq. (40), it is evident that to have a bound state at the interface, the vector β must belong to the null space of the reduced matrix A_r, defined to be the $S_g^{SC}\times S_g^M$ upper left part of the original matrix A. This follows since the matrices PE_M and E_{SC} were chosen to have the eigenstates with the largest eigenvalues as column vectors to the left. Thus, when the two subspaces S_g^{SC} and S_g^M have the same dimension, a bound state at the interface is characterized by the vanishing of the determinant of A_r. The bound state criterion is

$$\det A_r = 0. \tag{41}$$

This is the criterion used previously by Andersen and Hedegard to study the splitting of the ZES near dSC-AF interfaces.[24]

In Fig. 18, we show the results of Eq. (41) for the (100) [Fig. 18(a)] and (110) [Fig. 18(b)] AF/sSC interface, respectively. Here, we used a nested band $\mu=0.0$ with $M=0.4$ and $\Delta=0.1t$. In both graphs we also plot the curves given by the analytical results in Eqs. (33), (28), and (30), respectively. The (almost) complete overlap of the curves reveal that the transfer matrix method captures the low-energy bound states, and that these have the same dispersion as discussed in the previous sections. Small deviations are seen near the Brillouin zone edges. This is expected since the Fermi velocity v_F vanishes there and the quasiclassical approximation used to derive Eqs. (33) and (28) becomes less reliable.

For the AF/dSC interfaces we find similar agreement between the analytical results and the transfer matrix method.

V. THE AF/N/AF JUNCTION

Discrete quasiparticle bound states below the AF gap induced by Q reflection processes at AF/N interfaces exist in a planar AF/N/AF junction analogous to Andreev bound states in SC/N/SC systems.[25] Here, we present the analytical solution of the problem for the simple case $\Delta_s, m \ll v_{F,x}/a$, when the sublattice quasiclassical approximation applies well to both the superconductor and the antiferromagnet. Analogous to the Andreev Equations (20), we formulate Schrödinger equations for electrons with the quasiclassical approximation in the $(\boldsymbol{k}_F, \boldsymbol{k}_F+\boldsymbol{Q})$ representation,

$$\left(-iv_{F,x}(\boldsymbol{k}_F)\frac{\partial}{\partial x} - \mu - E\right)\tilde{u}_{\sigma,\boldsymbol{k}_F}(x) + \sigma m_{\pm}\tilde{u}_{\sigma,\boldsymbol{k}_F+\boldsymbol{Q}}(x) = 0,$$

$$\left(iv_{F,x}(\boldsymbol{k}_F)\frac{\partial}{\partial x} - \mu - E\right)\tilde{u}_{\sigma,\boldsymbol{k}_F+\boldsymbol{Q}}(x) + \sigma m_{\pm}\tilde{u}_{\sigma,\boldsymbol{k}_F}(x) = 0. \tag{42}$$

The relation $v_{F,x}(\boldsymbol{k}_F+\boldsymbol{Q}) = -v_{F,x}(\boldsymbol{k}_F)$ is taken into account in Eq. (42).

Let θ be a misorientation angle between two magnetic order parameters $\boldsymbol{m}_{\pm}$ in the right $x>d/2$ and the left $x<-d/2$ antiferromagnetic half spaces. Consider the magnetizations lying in the yz plane, which is perpendicular to the interface normal. The quasiparticle spin will be not a good quantum number in the case $\theta\neq 0,\pi$, so that we have to explicitly introduce spin coordinates. We choose the global quantization axis along the magnetization in the left antiferromagnet. Since Eqs. (42) are written for the quantization axis taken along the order parameters $m_{\pm}>0$, the solutions in the right antiferromagnet should be rotated by the angle θ around the x axis in spin space before matching them with the corresponding solution in the normal metal region at $x=d/2$. After the rotation, the low-energy solutions of Eqs. (42) in the right antiferromagnetic half space can be written as

$$\left[D_{+,\uparrow} \begin{pmatrix} \cos(\theta/2)e^{i\,\mathrm{sgn}(v_{F,x})\varphi_+} \\ i\sin(\theta/2)e^{i\,\mathrm{sgn}(v_{F,x})\varphi_+} \\ \cos(\theta/2) \\ i\sin(\theta/2) \end{pmatrix} + D_{+,\downarrow} \begin{pmatrix} -i\sin(\theta/2)e^{i\,\mathrm{sgn}(v_{F,x})\varphi_+} \\ -\cos(\theta/2)e^{i\,\mathrm{sgn}(v_{F,x})\varphi_+} \\ i\sin(\theta/2) \\ \cos(\theta/2) \end{pmatrix} \right] \exp\left(-\frac{\sqrt{m_+^2-(E+\mu)^2}}{|v_{F,x}|}x \right). \tag{43}$$

Here, we have introduced the notation

$$e^{i\varphi_\pm(E)} = \frac{1}{m_\pm}[E+\mu+i\sqrt{m_\pm^2-(E+\mu)^2}]. \tag{44}$$

The upper two lines in Eq. (43) describe the spin up and down amplitudes with the momentum $\boldsymbol{k}_F$ and the lower two lines show the relative values of spin up and down amplitudes with the momentum $\boldsymbol{k}_F+\boldsymbol{Q}$. The solutions for the left antiferromagnetic half space can be obtained from Eq. (43) after the substitutions $\theta\to 0$, $m_+\to m_-$, $\varphi_+\to-\varphi_-$, $D_{+,\uparrow(\downarrow)}\to D_{-,\uparrow(\downarrow)}$, $x\to -x$.

In the normal-metal region $-d/2<x<d/2$ the magnetization vanishes and the solutions of Eqs. (42) take the form

$$\begin{pmatrix} \tilde{u}_{\uparrow,\boldsymbol{k}_F}(x) \\ \tilde{u}_{\downarrow,\boldsymbol{k}_F}(x) \\ \tilde{u}_{\uparrow,\boldsymbol{k}_F+\boldsymbol{Q}}(x) \\ \tilde{u}_{\downarrow,\boldsymbol{k}_F+\boldsymbol{Q}}(x) \end{pmatrix} = \left[C_1 \begin{pmatrix} 1\\0\\0\\0 \end{pmatrix} + C_3 \begin{pmatrix} 0\\1\\0\\0 \end{pmatrix} \right] e^{ix(E+\mu)/v_{F,x}} + \left[C_2 \begin{pmatrix} 0\\0\\1\\0 \end{pmatrix} + C_4 \begin{pmatrix} 0\\0\\0\\1 \end{pmatrix} \right] e^{-ix(E+\mu)/v_{F,x}}. \tag{45}$$

In the absence of potential barriers, the quasiclassical solutions are continuous across the interfaces. Matching the solutions (43) and (45) at $x=\pm d/2$, we obtain the following equation for bound state energies:

$$E_n^\pm = \frac{|v_{F,x}|}{2d}(\varphi_+(E_n^\pm)+\varphi_-(E_n^\pm)\pm\theta+2\pi n)-\mu, \tag{46}$$

where $n=0,\pm1,\pm2,\cdots$.

The dependence of the bound state energies on the particular values $m_\pm$ disappears for low-energy states in the almost half filled lattice. Indeed, under the condition $|E_n+\mu| \ll m_\pm$ one can take $\varphi_\pm\approx\pi/2$ and find from Eq. (46) the following low-energy equidistant spectrum:

$$E_n^\pm(\boldsymbol{k}_F,\theta) = \frac{|v_{F,x}(\boldsymbol{k}_F)|}{2d}\left[2\pi\left(n+\frac{1}{2}\right)\pm\theta\right]-\mu. \tag{47}$$

As seen from Eq. (47), $E_{n+1}-E_n=\pi|v_{F,x}|/d$ and $E_n^\pm(\pi)-E_n(0)=\pm\pi|v_{F,x}|/2d$. The condition $|E_n+\mu|\ll m_\pm$ is valid for sufficiently large thickness of the normal-metal region $d\gg(\hbar v_{F,x}/m)\sim\xi_m$, when there can be many levels described by Eq. (47). The zero-energy bound state appears, in particular, in the half-filled lattice for $\theta=\pi$ when the relative phase of the antiferromagnetic ordering differs by π in the left and the right half spaces.

The spectrum (47) qualitatively differs from that in a conventional "particle in a box," i.e., a system of almost free quasiparticles confined by impenetrable walls constituting an $I/N/I$ junction. The reason for the difference is associated with strong correlations between electrons with momenta $\boldsymbol{k}_F$ and $\boldsymbol{k}_F+\boldsymbol{Q}$, induced in the normal-metal region by the antiferromagnets, where equations for electrons with $\boldsymbol{k}_F$ and $\boldsymbol{k}_F+\boldsymbol{Q}$ are coupled [see Eqs. (42)].

After the substitution $m_\pm\to\Delta$ the bound state energies (46) coincide with those obtained many years ago for SC/N/SC systems (at $\mu=0$) with the phase difference θ.[59] The reason for this is seen at $\theta=0$ where the quasiclassical equations (42) for electrons with momenta $\boldsymbol{k}_F$ and $\boldsymbol{k}_F+\boldsymbol{Q}$ coincide with the Andreev equations with $\mu=0$ and real Δ after the substitutions $\sigma m\to\Delta$, $\tilde{u}_{\sigma,\boldsymbol{k}_F+\boldsymbol{Q}}(x)\to\tilde{v}_{\bar{\sigma},\boldsymbol{k}_F}(x)$. It is important for this property that electrons with the momentum $\boldsymbol{k}_F+\boldsymbol{Q}$ possess a reverse velocity (similar to holes with the momentum $\boldsymbol{k}_F$) compared with electrons with the momentum $\boldsymbol{k}_F$. In the presence of a misorientation angle, one can transform Eqs. (42) into the corresponding Andreev equations at $\mu=0$ with complex Δ, if one uses a gauge transformation after rotating all the quantities in Eq. (42) over the angle θ in spin space.

In the following, we study the AF/N/AF junction from the solution of the BdG equations (4). For the coupling constants we have the following simple spatial dependence:

$$U_i = U \quad \text{for } |i|>\frac{d}{2}, \tag{48}$$

$$V_i = 0 \quad \text{for all } i, \tag{49}$$

and $U=0$ within the normal region $|i|\leqslant d/2$.

In Fig. 19 we plot the eigenbands for the (100) AF/N/AF junction when $\mu=0$, $U=2.7t$, $d=4$ [Fig. 19(a)] and $U=2.0t$, $d=48$ [Fig. 19(b)]. In the limit of a long normal region, we see that outside the parabola-shaped region centered at $k_y=0.0$, the bands roughly approach a set of equidistant sine-shaped bands, in agreement with Eq. (47) at $\theta=0$ for the (100) orientation. In this limit the low-energy LDOS in the N region (not shown) displays the expected equally spaced peaks. Note, that inside the parabola region we observe a qualitatively new dispersive behavior of the eigenenergies with maximum at $k_y=0$. We expect these deviations from the simple result of the quasiclassical treatment to be caused by the assumption $m\ll t$ used to obtain Eq. (47). In addition, the details of the spectrum near points where $v_{F,x}$ approaches zero can always differ from the quasiclassical result.

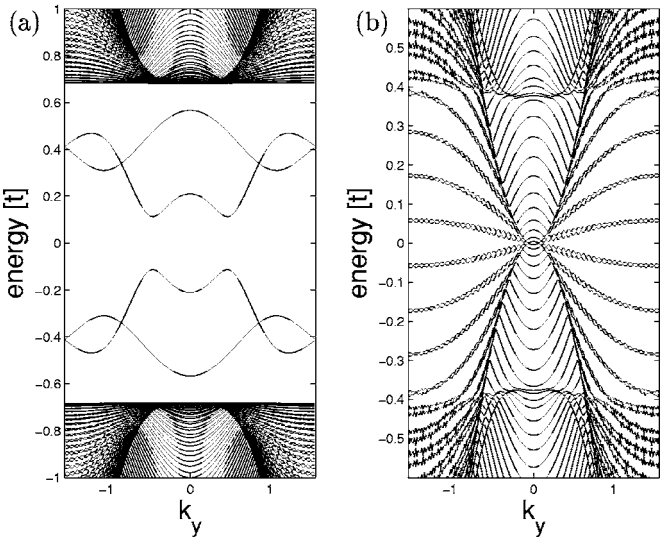

FIG. 19. Bound state eigenbands for a (100) AF/N/AF junction where the length d of the normal region N is either $d=4$ (a) or $d=48$ (b) lattice sites. Parameters: $\mu=0$, $U=2.7t$ (a), and $U=2.0t$ (b).

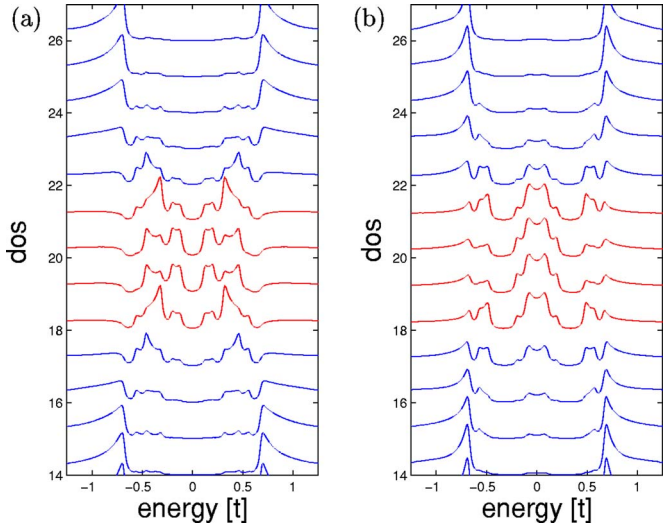

FIG. 20. (Color online) LDOS for the (100) AF/N/AF (a) and AF/N/πAF (b) junction with $d=4$, $\mu=0$, and $U=2.7t$. The four center LDOS scans are in the N region.

It is clear from Fig. 19(a) that we can have very strong deviations from the quasiclassical result when $d\sim a$ and $m\sim t$. In particular, within the quasiclassical framework the dispersion of the bound state energies is entirely associated with the momentum dependence of the Fermi velocity $v_{F,x}(\boldsymbol{k}_F)$. In contrast, Fig. 19(a) displays a more complicated momentum dependence of the energy levels with numerous extrema and additional peaks in the associated LDOS.

We have also studied a *spin-π junction*, a AF/N/πAF junction with $\theta=\pi$, where the magnetization has gained an extra π phase shift when crossing the normal region N. This is similar to the π-phase shift in the stripe phase of the cuprate superconductors.[60–62] For the AF/N/πAF junction the subgap bands are shifted compared to the AF/N/AF configuration. As a consequence, the associated LDOS will reveal whether the junction exhibits the π phase shift or not. This can be seen in Fig. 20 which shows the LDOS associated with Fig. 19(a) and the corresponding AF/N/πAF junction in Fig. 20(b). The surprisingly large number of peaks seen in Fig. 20 agree with the strongly dispersive bands as can be verified from the stationary points in Fig. 19(a). The presence of low-energy states seen in the AF/N/πAF junction in Fig. 20(b) correlates with predictions of the quasiclassical approach, which, however, does not apply directly to the case of very thin normal metal region $d=4$.

Figure 21 shows the bands and LDOS for the (110) AF/N/AF [Figs. 21(a) and 21(c)] and AF/N/πAF [Figs. 21(b) and 21(d)] junction, respectively. In accordance with Eqs. (46) and (47), the orientational dependence of the spectrum is associated with the Fermi velocity dispersion. Indeed, in the limit of large d, the bound state spectrum consists again of equidistant states like in the (100) case. For the (110) geometry we also find that the main qualitative difference between the AF/N/AF and AF/N/πAF junctions is associated with the presence of almost zero energy states in the latter case.

VI. CONCLUSIONS

We have performed a theoretical study of interfaces and junctions involving antiferromagnets and superconductors or normal metals. This was presented both in the framework of quasiclassics and self-consistent numerical solutions of the relevant Bogoliubov–de Gennes equations. Where comparison is appropriate, we found full agreement between the two methods. In particular, we investigated the formation of bound states near (100) and (110) interfaces between antiferromagnets and s- or d-wave superconductors. We calculated their dispersion, their influence on the proximity effect, and the associated modifications of the LDOS near the interface

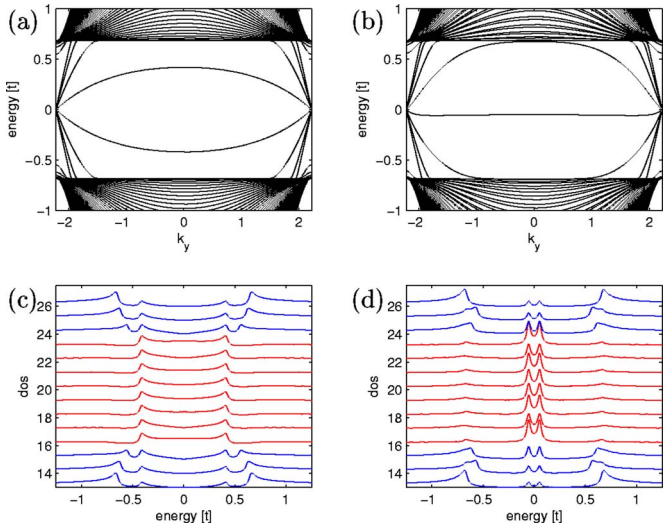

FIG. 21. (Color online) Eigenbands and the associated LDOS for the (110) AF/N/AF (a) and (c) and (110) AF/N/πAF (b) and (d) junction with $d=8$, $\mu=0$, and $U=2.7t$. Note the low-energy state generated in the spin-π junction. In the LDOS plots, the middle eight scans are in the N region whereas the upper and lower three shows the LDOS upon moving into the AF.

regions. In addition we discussed the crossover between Q reflection and conventional specular reflection as a function of the potential barrier at the interface. In future work we plan to investigate the role of the bound states on the Josephson current in SC/AF/SC junctions where the low-energy bound states can be expected to generate, e.g., unusual temperature dependence of the critical current.

ACKNOWLEDGMENTS

This work was supported by Grant No. NSF-INT-0340536 (I.V.B., P.J.H., and Yu.S.B.), U.S. DOE DE-FG02-05ER46236 (P.J.H. and Yu.S.B.), and by ONR Grant No. N00014-04-0060 (P.J.H and B.M.A). I.V.B. and Yu.S.B. also acknowledge the support by Grant No. RFBR 05-02-17175.

[1] I. Zutić, J. Fabian, and S. Das Sarma, Rev. Mod. Phys. **76**, 323 (2004).
[2] V. V. Ryazanov, V. A. Oboznov, A. Yu. Rusanov, A. V. Veretennikov, A. A. Golubov, and J. Aarts, Phys. Rev. Lett. **86**, 2427 (2001).
[3] T. Kontos, M. Aprili, J. Lesueur, F. Genêt, B. Stephanidis, and R. Boursier, Phys. Rev. Lett. **89**, 137007 (2002).
[4] W. Guichard, M. Aprili, O. Bourgeois, T. Kontos, J. Lesueur, and P. Gandit, Phys. Rev. Lett. **90**, 167001 (2003).
[5] A. Bauer, J. Bentner, M. Aprili, M. L. Della-Rocca, M. Reinwald, W. Wegscheider, and C. Strunk, Phys. Rev. Lett. **92**, 217001 (2004).
[6] A. I. Buzdin, L. N. Bulaevsky, and S. V. Panyukov, Pis'ma Zh. Eksp. Teor. Fiz. **35**, 147 (1982) [JETP Lett. **35**, 178 (1982)].
[7] A. I. Buzdin, B. Bujicic, and M. Yu. Kupriyanov, Zh. Eksp. Teor. Fiz. **101**, 231 (1992) [Sov. Phys. JETP **74**, 124 (1992)].
[8] N. M. Chtchelkatchev, W. Belzig, Yu. V. Nazarov, and C. Bruder, Pis'ma Zh. Eksp. Teor. Fiz. **74**, 357 (2001) [JETP Lett. **74**, 323 (2001)].
[9] Yu. S. Barash and I. V. Bobkova, Phys. Rev. B **65**, 144502 (2002); M. Fogelstom, *ibid.* **62**, 11812 (2000).
[10] S. Yu. Barash, I. V. Bobkova, and T. Kopp, Phys. Rev. B **66**, 140503(R) (2002).
[11] I. Bozovic, G. Logvenov, M. A. J. Verhoeven, P. Caputo, E. Goldobin, and T. H. Geballe, Nature (London) **422**, 873 (2003).
[12] H. Kotegawa, Y. Tokunaga, Y. Araki, G.-Q. Zheng, Y. Kitaoka, K. Tokiwa, K. Ito, T. Watanabe, A. Iyo, Y. Tanaka, and H. Ihara, Phys. Rev. B **69**, 014501 (2004).
[13] H. Hilgenkamp and J. Mannhart, Rev. Mod. Phys. **74**, 485 (2002).
[14] S. Katano, M. Sato, K. Yamada, T. Suzuki, and T. Fukase, Phys. Rev. B **62**, R14677 (2000).
[15] B. Lake, G. Aeppli, K. N. Clausen, D. F. McMorrow, K. Lefmann, N. E. Hussey, N. Mangkorntong, M. Nohara, H. Takagi, T. E. Mason, and A. Schroder, Science **291**, 1759 (2001).
[16] V. F. Mitrovic, E. E. Sigmund, M. Eschrig, H. N. Bachman, W. P. Halperin, A. P. Reyes, P. Kuhns, and W. G. Moulton, Nature (London) **413**, 501 (2001).
[17] D. P. Arovas, A. J. Berlinsky, C. Kallin, and S. C. Zhang, Phys. Rev. Lett. **79**, 2871 (1997).
[18] B. M. Andersen, H. Bruus, and P. Hedegard, Phys. Rev. B **61**, 6298 (2000).
[19] E. Demler, A. J. Berlinsky, C. Kallin, G. B. Arnold, and M. R. Beasley, Phys. Rev. Lett. **80**, 2917 (1998).
[20] H. Zabel, J. Phys.: Condens. Matter **11**, 9303 (1999).
[21] K. Miyagawa, A. Kawamoto, and K. Kanoda, Phys. Rev. Lett. **89**, 017003 (2002).
[22] C. Bell, E. J. Tarte, G. Burnell, C. W. Leung, D.-J. Kang, and M. G. Blamire, Phys. Rev. B **68**, 144517 (2003).
[23] L. P. Gor'kov and V. Kresin, Appl. Phys. Lett. **78**, 3657 (2001).
[24] B. M. Andersen and P. Hedegard, Phys. Rev. B **66**, 104515 (2002).
[25] I. V. Bobkova, P. J. Hirschfeld and Yu. S. Barash, Phys. Rev. Lett. **94**, 037005 (2005).
[26] E. Fawcett, Rev. Mod. Phys. **60**, 209 (1988).
[27] E. Fawcett, H. L. Alberts, V. Yu. Galkin, D. R. Noakes, and J. V. Yakhmi, Rev. Mod. Phys. **66**, 25 (1994).
[28] A. W. Overhauser, Phys. Rev. **128**, 1437 (1962).
[29] C. R. Hu, Phys. Rev. Lett. **72**, 1526 (1994).
[30] Y. Tanaka and S. Kashiwaya, Phys. Rev. Lett. **74**, 3451 (1995).
[31] L. J. Buchholtz, M. Palumbo, D. Rainer, and J. A. Sauls, J. Low Temp. Phys. **101**, 1099 (1995).
[32] Y. Tanuma, Y. Tanaka, M. Yamashiro, and S. Kashiwaya, Phys. Rev. B **57**, 7997 (1998).
[33] A. F. Andreev, Zh. Eksp. Teor. Fiz. **46**, 1823 (1964) [Sov. Phys. JETP **19**, 1228 (1964)].
[34] A. Shelankov, JETP Lett. **32**, 111 (1980); Sov. Phys. Solid State **26**, 981 (1984).
[35] V. S. Shumeiko, E. N. Bratus', and G. Wendin, Low Temp. Phys. **23**, 181 (1997); V. S. Shumeiko, G. Wendin, and E. N. Bratus', Phys. Rev. B **48**, 13129 (1993).
[36] I. V. Bobkova and Yu. S. Barash, Phys. Rev. B **71**, 144510 (2005).
[37] J. Tersoff and D. R. Hamann, Phys. Rev. B **31**, 805 (1985).
[38] Z. Radović, M. Ledvij, L. Dobrosavljević-Grujić, A. I. Buzdin, and J. C. Clem, Phys. Rev. B **44**, 759 (1991).
[39] E. A. Demler, G. B. Arnold, and M. R. Beasley, Phys. Rev. B **55**, 15174 (1997).
[40] P. Fulde and A. Ferrell, Phys. Rev. **135**, A550 (1964); A. Larkin and Y. Ovchinnikov, Sov. Phys. JETP **20**, 762 (1965).
[41] I. V. Bobkova and Yu. S. Barash, JETP Lett. **80**, 494 (2004).
[42] J. Lesueur, L. H. Greene, W. L. Feldmann, and A. Inam, Physica C **191C**, 325 (1992).
[43] M. Covington, R. Scheuerer, K. Bloom, and L. H. Greene, Appl. Phys. Lett. **68**, 1717 (1996).
[44] M. Covington, M. Aprili, E. Paraoanu, L. H. Greene, F. Xu, J. Zhu, and C. A. Mirkin, Phys. Rev. Lett. **79**, 277 (1997).
[45] L. Alff, H. Takashima, S. Kashiwaya, N. Terada, H. Ihara, Y. Tanaka, M. Koyanagi, and K. Kajimura, Phys. Rev. B **55**, R14757 (1997).
[46] J. W. Ekin, Y. Xu, S. Mao, T. Venkatesan, D. W. Face, M. Eddy, and S. A. Wolf, Phys. Rev. B **56**, 13746 (1997).
[47] M. Aprili, M. Covington, E. Paraoanu, B. Niedermeier, and L. H. Greene, Phys. Rev. B **57**, R8139 (1998).
[48] L. Alff, S. Kleefisch, U. Schoop, M. Zittartz, T. Kemen, T. Bauch, A. Marx, and R. Gross, Eur. Phys. J. B **5**, 423 (1998).

[49] L. Alff, A. Beck, R. Gross, A. Marx, S. Kleefisch, Th. Bauch, H. Sato, M. Naito, and G. Koren, Phys. Rev. B **58**, 11197 (1998).
[50] S. Sinha and K.-W. Ng, Phys. Rev. Lett. **80**, 1296 (1998).
[51] J. Y. T. Wei, N.-C. Yeh, D. F. Garrigus, and M. Strasik, Phys. Rev. Lett. **81**, 2542 (1998).
[52] M. Aprili, E. Badica, and L. H. Greene, Phys. Rev. Lett. **83**, 4630 (1999).
[53] R. Krupke and G. Deutscher, Phys. Rev. Lett. **83**, 4634 (1999).
[54] M. Covington and L. H. Greene, Phys. Rev. B **62**, 12440 (2000).
[55] I. Iguchi, W. Wang, M. Yamazaki, Y. Tanaka, and S. Kashiwaya, Phys. Rev. B **62**, R6131 (2000).
[56] L. H. Greene, P. Hentges, H. Aubin, M. Aprili, E. Badica, M. Covington, M. M. Pafford, G. Westwood, W. G. Klemperer, S. Jian, and D. G. Hinks, Physica C **387**, 162 (2003).
[57] Y. Ohashi, Phys. Rev. B **60**, 15388 (1999).
[58] C. Honerkamp, K. Wakabayashi, and M. Sigrist, Europhys. Lett. **50**, 368 (2000).
[59] I. O. Kulik, Zh. Eksp. Teor. Fiz. **57**, 1745 (1969) [Sov. Phys. JETP **30**, 944 (1969)].
[60] J. M. Tranquada, B. J. Sternlieb, J. D. Axe, Y. Nakamura, and S. Uchida, Nature (London) **375**, 561 (1995).
[61] J. Zaanen and O. Gunnarsson, Phys. Rev. B **40**, R7391 (1989); D. Poilblanc and T. M. Rice, *ibid.* **39**, R9749 (1989); K. Machida, Physica C **158C**, 192 (1989); H. J. Schulz, J. Phys. (Paris) **50**, 2833 (1989).
[62] B. M. Andersen and P. Hedegard, Phys. Rev. Lett. **95**, 037002 (2005).